Theranostic role of Nanoparticles on cancer cells using Photothermal therapy

M.Sc. Thesis

By

SIMRAN

DEPARTMENT OF BIOSCIENCES AND BIOMEDICAL ENGINEERING

INDIAN INSTITUTE OF TECHNOLOGY INDORE

MAY 2024

Theranostic role of Nanoparticles on cancer cells using Photothermal therapy

A THESIS

Submitted in partial fulfillment of the
requirements for the award of the degree
of
Master of Science

by
SIMRAN

DEPARTMENT OF BIOSCIENCES AND BIOMEDICAL ENGINEERING

INDIAN INSTITUTE OF TECHNOLOGY INDORE

MAY, 2024

INDIAN INSTITUTE OF TECHNOLOGY INDORE

CANDIDATE'S DECLARATION

I hereby certify that the work which is being presented in the thesis entitled **'Theranostic role of nanoparticles on cancer cell using Photothermal therapy'** in the partial fulfillment of the requirements for the award of the degree of **MASTER OF SCIENCE** and submitted in the **DEPARTMENT OF BIOSCIENCES AND BIOMEDICAL ENGINEERING, Indian Institute of Technology Indore**, is an authentic record of my own work carried out during the time period from July 2022 to May 2024 under the supervision of Dr. Abhijeet Joshi, Associate Professor, Department of Biosciences and Biomedical Engineering.

The matter presented in this thesis has not been submitted by me for the award of any other degree of this or any other institute.

Simran 24/5/24

Signature of the student with date

Simran

This is to certify that the above statement made by the candidate is correct to the best of my/our knowledge.

AB Joshi 24/5/24

Signature of the Supervisor of thesis with date

DR. Abhijeet Joshi

Simran has successfully given his/her M.Sc. Oral Examination held on 9th May 2024.

AB Joshi 24/5/24

Signature(s) of Supervisor(s) of MSc thesis

Date:

P.V. Kodgire

Convener, DPGC

Date: 24/05/24

ACKNOWLEDGEMENTS

I commenced my journey here with almost zero prior knowledge or experience of working in any lab. This project would not get completed without the support of many members over here and for that I extend my honest gratitude towards each and every person who directly or indirectly taught me various things during this research project journey.

Firstly, I extend my gratitude towards my project instructor **Dr. Abhijeet Joshi** who never minded my silly mistakes and taught me every little thing required in any profession. In every meeting, he always promoted discussion on ideas whether about research or life. His calm and gentle nature is truly incredible by which I also learned lifelong skills. This has been an epic journey for me working under his supreme guidance. Without their guidance and persistent help, this project would not have been possible within the limited time frame.

Badri Narayana Sahoo who treated me as his sister and taught every single thing from lab techniques. I extend my honest gratitude to him as without him I cannot even think to complete this project journey of my master's. His expertise, dedication, and encouragement have shaped my research and my growth as a scholar and individual. Thank you for your patience, and for believing in my potential when I doubted myself.

I also extend my gratitude to **Dr. Sharad Gupta** for providing me IR thermal imaging camera.

I am grateful to my seniors **Surbhi Jaiswal** and **Tileshwar Sahare** for all their valuable lessons and help during all the experiments.

Heart thanks to **Anusha Srivastava** for all the scientific discussions and for keeping me motivated, energetic, and always for their kind support and valuable time.

I also extend my gratitude to other lab members **Dr. V. Sharan Rathnam** (NPDF) for being there for every kind of support and guidance.

A very special thanks to **Prof. Amit Kumar** as it was him who encouraged & motivated me to go for whatever I aspired.

I extend my gratitude to the **BSBE department** (Mr. Arif Patel, Mr. Gaurav Singh, and Mr. Amit Kumar) and SIC, IIT Indore, for the instrumentational facilities. A special thanks to **Mr. Atul Kumar** for teaching me the operation of SEM at SIC and **Ravindra Kumar** sir for his supportive and kind nature at the CLSM facility.

I am grateful to my friends **Vibha Choudhary**, **Bidisha Choudhary** and **Shivani Vaja** who have been my sides through thick and thin.

Heart thanks to **Pranit H. Bagde** for their support and encouragement during my research project.

I would like to express my deep gratitude to the source of my life, my parents (**Mr. Ranjeet Singh Rana** and **Mrs. Mamta Rana**) for their unconditional love, care and for making me capable enough to work. They have been a constant support to me. A hearty thanks to my sibling **Akanksha** for understanding me and always guiding and motivating me. Without them, I would not be here where I am today.

Dedicated to my Parents

Mr. Ranjeet Singh Rana,

Mrs. Mamta Rana

and my sibling

Akanksha

Abstract

Cancer is a deadly disease with millions of deaths annually. Enormous trials are going on towards preventing and curing this disease and developing various therapies. Using anti-cancer drugs freely causes several side effects on healthy cells. So, nanoparticles can be used for control and targeted drug delivery. The critical requirement for early disease identification and diagnosis drives the advancement of imaging techniques and contrast agents. Nanoparticle based bioimaging can also be done for bioimaging of cancer. Photothermal therapy is a widely used therapy for treating cancer in which NIR laser light is used to increase the temperature due to which cell death can occur. Various photo agents are used for PTT including NIR dyes. Iron oxide is widely used for photothermal therapy. So, in this project, the aim is to synthesize a theranostic nanohybrid using gold-coated iron oxide nanoparticles and chitosan for photothermal therapy as well as bioimaging using MRI and X-ray

LIST OF PUBLICATIONS

From thesis

- Theranostic role of Nanoparticles on cancer cells using Photothermal therapy – (Manuscript under preparation)

Apart from thesis

- Current status of Point-Of-Care Lateral flow tests for biomarker detection in kidney diseases (Tileshwar Sahare[1], Badri Narayana Sahoo[1], Surbhi Jaiswal[1], Simran Rana[1] & Abhijeet Joshi[1])
- Synergistic anticancer effect of Doxorubicin and Tamoxifen loaded in Chitosan nanoparticles towards ER-positive breast cancer therapy (Badri Narayana Sahoo[1] , Bhavana Joshi[1] , Simran Rana[1] , VS Sharan Rathnam[1] , Tileshwar Sahare[1], Abhijeet Joshi[1],)

TABLE OF CONTENTS

LIST OF FIGURES

LIST OF TABLES

NOMENCLATURE

Acronym	Expansion
Dox	Doxorubicin
NPs	Nanoparticles
PTT	Photothermal Therapy
IONP	Iron oxide nanoparticles
ROS	Reactive Oxygen Species
PLGA	Poly- (Lactic-co-glycol acid)
CQD	Carbon quantum dots
NIR	Near Infrared
FESEM	Field emission scanning electron microscopy
XRD	X-ray diffraction
DMSO	Dimethyl sulphoxide
MTT	(3-(4,5-dimethylthiazol-2-yl)-2,5-diphenyltetrazolium bromide) dye
DCFDA	2',7'-dichlorofluroscein diacetate dye
GF-AFC	Glycylphenlyalanyl-aminoflurocoumarin dye
PI	Propidium iodide dye
CLSM	Confocal laser scanning microscopy

ACRONYMS

Sign	Meaning
λ	Wavelength
µ	Micron
°C	Degree Centigrade
µl	Microlitre
ml	Millilitre
nm	Nanometer
nM	Nanomolar
µg/ml	Microgram per millilitre
mins	Minutes
hrs	Hours
R^2	Regression coefficient
W	Watt
%	Percentage

Chapter 1

Introduction

1.1 Cancer

1.1.1 Introduction

Globally, cancer is the leading cause of mortality. There are 14.1 million new cases and 8.2 million deaths were reported by the World Health Organization (Conde, 2018). Cells proliferate and divide out of control as a result of cancer. Tumor cells undergo a variety of alterations that give them the potential to penetrate nearby tissue, which leads to the spread of cancer to further tissues. When there is no safeguard against this form of division, the patient dies. Depending on the organs involved, there are several types of cancer. Cancer may be caused by exposure to carcinogenic substances such as chemical dyes, radiation, smoking, or epigenetic or genetic changes. Lung, breast, prostate, and colorectal cancer are the cancers that are most frequently diagnosed. Out of all cancers, liver, lung, and stomach, cancer caused the most fatalities.

1.1.2 Causes of cancer

Cancer is caused by sudden changes or mutations in DNA. It can be present by birth or can occur throughout life. Some mutations present by birth and inherited from parents which increases the risk of cancer. Whereas, some cancer occurs due to physical, chemical, and biological factors. The physical factors include UV or ionizing radiation. Chemical factors are carcinogenic drugs, alcohol, and tobacco, which can cause cancer. Some biological agents such as human papillomavirus and hepatitis B virus cause cancer.

1.1.3 Imaging techniques

Several imaging techniques are available such as X-ray imaging, optical imaging, Computed tomography (CT), Magnetic imaging resonance (MRI), Positron emission tomography (PET), Single photon emission computed tomography (SPECT), and ultrasound (Sharma et al., 2006).

MRI is based on the principle of nuclear magnetic resonance in which the NMR signals are generated by hydrogen nuclei located in organisms. In X-ray imaging, the machine sends X-ray radiation that passes through the body. The different parts of the body absorb different amounts of energy and give a different contrast to the image. Optical imaging is a non-invasive technique, which can create a contrast by wavelength, intensity, interference, and polarization. Different parameters of light interact with tissue and give the image. PET is a potent and popular nuclear medicine technique that has a high tissue penetration and a high degree of sensitivity. It can analyze quantitative imaging data in real time (Han et al., 2019a). With similar benefits to PET imaging, single photon emission computed tomography (SPECT) is another popular nuclear medicine method that can identify aberrant metabolic functions before changes in anatomy (Han et al., 2019b). However, PET and SPECT techniques have side effects due to the radioactive exposure, and therefore the quantum dots can be used for imagining because of their biocompatibility and stability in tissues.

1.1.4 Current treatment and strategies

a) Chemotherapy

It is a technique that is used to stop the tumor progression by destroying their ability to divide and causing them to undergo apoptosis. Cytotoxic chemicals are used to reduce or kill cancer cells. However, has some drawbacks as it may inhibit the growth of other fast-dividing cells like bone marrow cells, hair follicles, and gastrointestinal cells. This leads to several side effects like hair loss, bowel problems, and nausea (Salem et al., 2018).

b) Radiation therapy

In radiation therapy high doses of radiation are used to shrink and kill cancer cells. Radiation therapy is effective for various types of cancer like breast cancer, prostate, lung, head, and neck cancer. Depending upon the type and stage of cancer, radiation therapy can also be used with other

therapies like surgery or chemotherapy (Brannon-Peppas & Blanchette, 2004). It also has some side effects such as fatigue, skin irritation, and gastrointestinal issues (Baumann et al., 2016).

c) Surgical methods

Surgery is a common method of removing the cancerous organ or tissue from the body. It is a highly effective method when the cancer does not spread to the other tissue. Surgery can be highly effective when the cancer is localized and has not spread to other organs. But it also has side effects like bleeding, damage to nearby tissues or organs, and infection.

d) Photothermal and Photodynamic therapy

Photothermal therapy uses a photothermal agent which absorbs laser light due to which there is a temperature rise and cell death can occur. Whereas photodynamic therapy involves photosensitizers that absorb NIR laser light and produce toxic singlet oxygen or free radicles hence, cell destruction can occur (Huang et al., 2008).

1.2 Nanoparticles in health care

Nanotechnology products have been becoming useful in healthcare which results in the development of nanocarriers for the diagnosis, imaging, and treatment of a variety of diseases, including cancer, central nervous system, ophthalmic, and cardiovascular ailments. The primary goal is to deliver a drug and release it in a controlled manner at a particular site like cancer cells or tissue. This can be achieved by the nanoparticles. The nanoparticles are small colloidal molecules having a size from 1 nm to 1000 nm. It is used for the delivery of a drug in site specific manner, in which the drug is encapsulated or attached to the matrix of nanoparticles. So, this minimizes the loss of drug and side effects (Mohanraj & Chen, 2006). Depending on the preparation process, nanoparticles can also be divided into nanocages, nanospheres, nanorods, and nanocapsules. The nanoparticles should be highly biodegradable, and highly biocompatible, with minimum toxicity as well as stable accumulation in the target tissue

used for drug delivery. The nanoparticles are classified into four different types.

i. Liposomes are lipid-based vesicles that are used for targeted drug delivery. Depending upon the physiochemical property, the drug is intercalated into a lipid bilayer or entrapped into the aqueous space of liposome and delivered actively or passively.
ii. Polymeric nanoparticles which have a great potential for targeted drug delivery. In this, the drug or any other active compound is entrapped or absorbed into the polymeric core. The advantage of using polymeric nanoparticles is that they can control drug release. PLGA and chitosan are examples of polymeric nanoparticles.
iii. Inorganic nanoparticles which consist of metal and metal oxides. These nanoparticles offer different types of properties like conductivity, and thermal and magnetic properties which makes them valuable in different fields. The most common examples are iron oxide, gold, and silver nanoparticles and they are used for imaging as well as photothermal therapy.
iv. Carbon-based nanoparticles are made up of carbon atoms that are arranged in different structures that give them unique properties. They have electrical conductivity, high strength, and electron affinity. Fullerenes, carbon dots, and graphene are some examples.

1.2.1 Nanoparticles for Bioimaging

At present, nanoparticles are used for tumor diagnosis as well as therapeutic purposes due to their small size and biocompatibility such as gold, iron oxide, and quantum dots.

The X-ray and computed tomography (CT)-scan uses X-rays for the detection of tumors and provides a contrasting image by X-ray attenuation between soft tissues and highly dense bones or cancerous tissues. In order to enhance the contrast between normal and malignant

tissues, CT contrasting agents such as small organic iodinated compounds are used which have some limitations such as fast clearance, renal toxicity, and in adverse conditions anaphylaxis. So, to overcome this, nanoparticles can be used for CT scan such as metal-based nanoparticles. Gold nanoparticles are widely used for the detection of tumors by X-ray and CT scan due to their high atomic number and hence act as a better contrasting agent than iodinated compounds. It has greater X-ray absorption efficiency and is biocompatible.

Magnetic resonance imaging is an imaging technique that uses a strong magnetic field to generate images of organs. The contrasting agents (CAs) are used to enhance the contrast to differentiate the normal tissue and cancerous tissues. Gadolinium complexes are a contrasting agent but it is toxic, especially to patients suffering from kidney diseases. To overcome this, Superparamagnetic iron oxide (SPION) nanoparticles are highly used for MRI imaging.

Carbon quantum dots (CQD) are used for cell imaging and have ultra-small sizes, of less than 10 nm. They are bio-compatible, photothermal stable low cost & and less toxicity and therefore a promising future in the biological field. Cells can quickly acquire CQDs, and one or more photon excitations can be used to image them. A carbon quantum dot is a unique member of the carbon materials family and has lately been widely utilized for fluorescent bioimaging and theranostics due to its outstanding stability, cytocompatibility, and fluorescence properties. Numerous studies have demonstrated that CQDs are less cytotoxic than other QDs (Shen et al., 2022).

1.2.2 Nanoparticles for Photothermal Therapy

Photothermal therapy is a promising cancer treatment technique that causes cell death by producing heat in tumor tissues when exposed to laser light. Photothermal therapy mediated by NPs has emerged as a promising cancer treatment technique that has been used to treat a variety of malignant cell lines (Curry et al., 2013).

In photothermal therapy, the nanoparticles or photo agents absorb near-infrared (NIR) light (650-1350 nm) and induce a therapeutic response. As a result, hyperthermia is produced by photothermal agents in response to NIR light irradiation, and hence due to an increase in temperature, there is a denaturation of protein and cell death. This is the basis of photothermal therapy. Through thermal ablation, PTT may reduce tumor burden, which makes it an attractive choice for cancer treatment. Hyperthermia (>42 °C) produced by photothermal agents can kill cancer cells by fragmenting the cell membrane, harming the cytoskeleton, and preventing DNA synthesis by applying localized NIR light irradiation (Huang et al., 2021).

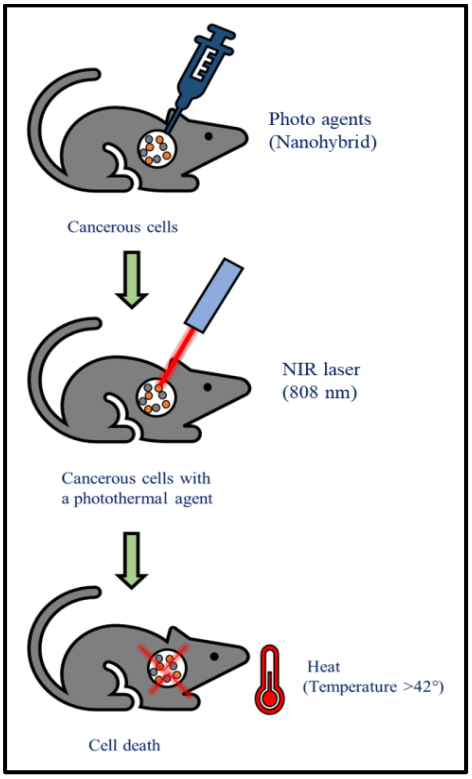

Figure 1.1: Mechanism of Photothermal therapy by exposing photo-agents with NIR laser

The chemistry behind the photothermal therapy is, that on absorbing light, the electron of photo agents shifts from low energy ground state to high energy excited state. The electronic excitation energy subsequently relaxes through nonradiative decay channels and hence there is an increase in kinetic energy which overall leads to the overheating of the tissue environment (Huang et al., 2008). Due to the overheating of the environment, the death of cells and tissue started due to the fragmentation of the cell membrane, the cytoskeleton is also disrupted and DNA synthesis is prevented.

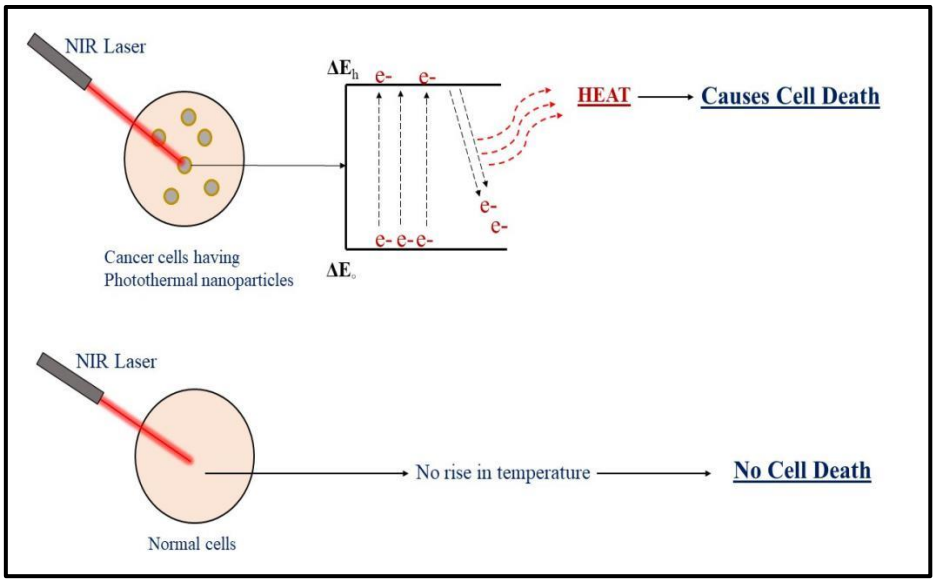

Figure 1.2: Chemistry behind photothermal therapy by exposing photo agents with NIR laser

1.2.3 Doxorubicin in cancer therapy

Doxorubicin drug was extracted from streptomyces and is used in the treatment of various types of cancer such as lung, breast, gastric, ovarian cancers, and lymphoma. It is an anthracycline drug that interacts with DNA by intercalation and inhibits the synthesis of macromolecules.

Doxorubicin also interacts with the progression of the topoisomerases II enzyme, which relaxes the super-coiling of DNA for transcription and also generates free radicle that induces DNA and cell membrane damage (Thorn et al., 2011). However, this chemotherapeutic drug possesses cytotoxicity leading to some adverse side effects in different organs such as the kidney, heart, brain, and liver. Therefore, different strategies have been developed to decrease the side effects of this drug such as its lack of solubility with poor distribution and destroying normal cells along with cancerous cells due to its non-specificity.

Chapter 2

Literature Review

Photothermal therapy was a great approach to treating cancer (Huang et al., 2008). The heat generated by exposing photothermal agents with NIR laser only targets the cancerous cells without damaging nearby healthy tissues (Fu et al., 2020). Various types of photothermal agents are there such as magnetic nanoparticles which include iron oxide, gold, and silver, then dyes also act as photothermal agents like ICG and methylene blue. Magnetic nanoparticles were widely used for photothermal therapy due to their property to produce heat on exposure to light such as iron, gold, copper, zinc, etc. The iron oxide nanoparticles were used for photothermal therapy because they absorb NIR light and induce a therapeutic response (Estelrich & Busquets, 2018). The iron oxide nanoparticles were used with polymers for photothermal therapy (Yang et al., 2017). The cytotoxicity of iron particles was checked and it was found that it doesn't show any harmful effect. It is bio-compatible. The polymeric magnetic nanoparticles were theranostic nanoparticles that were used for drug delivery as well as for bioimaging purposes for brain tumors (Joshi and Joshi 2022). Another study uses photothermal therapy for treating hepatocellular carcinoma using positively charged chitosan-coated gold nanoparticles (Salem et al., 2018). The NIR-absorbing organic dyes were used for photothermal therapy and imaging (Zhou et al., 2016). So, according to the literature iron oxide nanoparticles were widely used for therapeutics as well as diagnosing purposes.

The chitosan was used for the delivery of Doxorubicin. The polymer was used for controlled drug release with an encapsulation efficiency of less than 50% (Joshi et al., 2020). The development of pH-sensitive nanoparticles for dox delivery has been an excellent approach in recent years. This is the reason, polymeric nanoparticles are used for drug delivery (Meng et al., 2014). The therapeutic drug was encapsulated

within biocompatible and biodegradable PLGA nanoparticles against glioblastoma which shows 53% encapsulation efficiency (Kaur et al., 2021).

Table 2.1 The various research studies on photothermal therapy by iron-oxide nanoparticles and drug delivery by Chitosan nanoparticles

Author	Nanoparticles used	Objective
(Fu et al., 2020)	Iron oxide nanoparticles	Fe_3O_4 nanoparticles were used for Photothermal therapy
(Joshi et al., 2023)	Chitosan loaded with Dox and iron oxide nanoparticles	Chitosan-based nanohybrids were formed for drug delivery and MRI.
(Joshi et al., 2020)	Chitosan loaded with Doxorubicin drug	The chitosan nanoparticles were used for pH-responsive drug delivery of Doxorubicin.
Kharey et al., 2023	Iron oxide and gold nanocomposites	Nanocomposites were used for Photothermal therapy and diagnostics by MRI.
Narayanan et al., 2012	Iron oxide and gold nanohybrid	Fe_3O_4/Gold nanohybrid was used for theranostic purposes.

Chapter 3

Materials and Methodology

3.1 Materials

Chitosan, sodium tripolyphosphate, Doxorubicin drug from TCI (Japan) acetone, glacial acetic acid, gold chloride from SRL, Ferric chloride from RANKEM chemicals, Iron sulfate from RANKEM chemicals, sodium citrate. 3-(4,5-Dimethylthiazol-2-yl)-2,5-Diphenyltetrazolium bromide (MTT), dimethyl sulphoxide (DMSO) from Sigma-Aldrich Chemicals Ltd. (St. Louis, MO, USA). Dulbecco's modified eagle media, antibiotic, Fetal Bovine Serum, Trypsin, PBS, and all other cell culture reagents, Propidium Iodide dye, Glycylphenylalanyl-aminocoumarin (GF-AFC dye), Hoechst dye for staining.

3.2 Methods

3.2.1 Synthesis of Iron oxide nanoparticles

The iron oxide nanoparticles were made by the co-precipitation method in which 1% $FeCl_3$ was mixed with 1% $FeSO_4$ in a beaker i.e., in a 2:1 ratio, and then placed on a magnetic stirrer at 500 -700 rpm. Then the pH was maintained at 12 by the addition of 5 M NaOH dropwise. After maintaining pH at 12, the suspension was boiled at 80-90º C for 2 hrs. The suspension was washed three times with absolute ethanol by centrifugation for 15 mins at 5000 g. The pellet obtained was then dried in a microwave oven overnight at 55º C. After it was dried completely, the pellet to make a powder and stored for further analysis (Joshi et al., 2020).

3.2.2 Synthesis of gold-coated iron oxide nanoparticles

100 mg of iron oxide nanoparticles were dispersed in distilled water (1 mg/ml) by using a probe sonicator and then placed on a magnetic stirrer. 10 mM $HAuCl_4$ was added and boiled at 80° C for 15 mins. 2 ml of 155 mM sodium citrate was added as a reducing agent and left for 15 mins. Then this solution was washed three times by centrifugation (Kubota centrifuge, japan) using distilled water for 15 mins at 5000-6000 g.

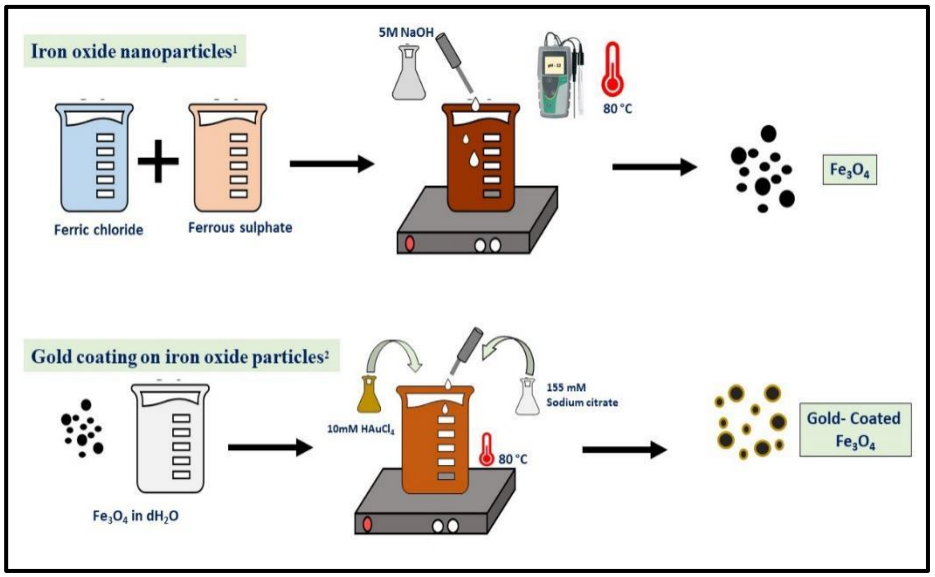

Figure 3.1: Diagrammatic representation of iron-oxide and gold-coated iron-oxide nanoparticles

3.2.3 Synthesis of Doxorubicin loaded with gold-coated iron oxide nanoparticles conjugated chitosan nanohybrids

This nanohybrid was synthesized by the ultrasonic atomizer. In a syringe, 0.5% (w/v) of chitosan was taken with 1 mg of Doxorubicin and 10 mg of gold-coated iron oxide nanoparticles. Then 1% (w/v) TPP (25 ml) was taken in a beaker and placed on a magnetic stirrer at 1500 rpm below the

nozzle of the atomizer. The mixture of chitosan, drug, and gold-coated iron particles was loaded in a syringe and pumped with a flow rate of 0.3 ml/min at a frequency of 130 kHz, and power of 3.5 watts. The droplets were collected in 1% (w/v) TPP which acts as a cross-linker (Joshi et al., 2020). After completion of spraying, the nanosuspension was centrifuged using ultracentrifuge at a speed of 30,000 g for 30 mins at 10º C. The supernatant was collected and washed the pellet thrice with distilled water. The pellet was stored for further analysis.

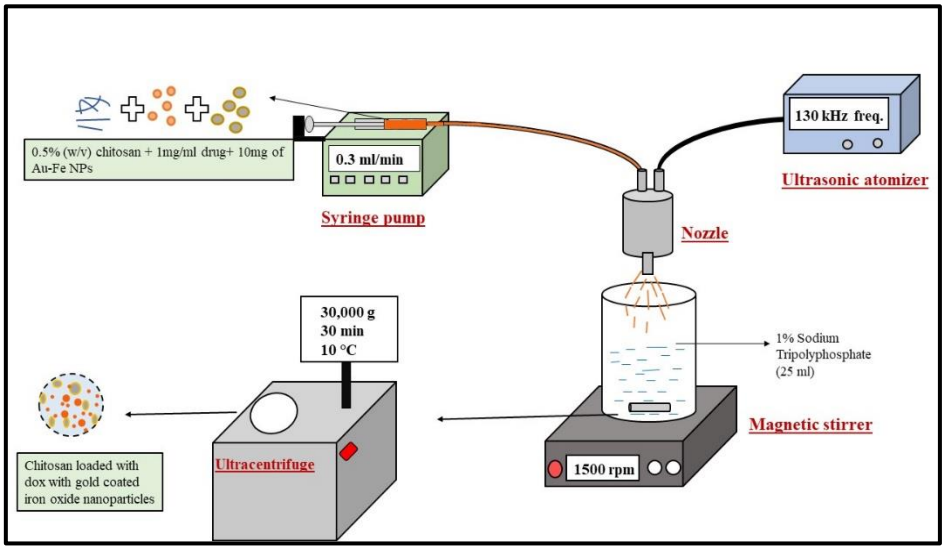

Figure 3.2: Diagrammatic representation of the synthesis of chitosan-loaded with Dox and gold-coated iron oxide nanoparticles

3.2.4 Preparation of calibration curve of drug

The calibration curve provides the linearity coefficient and regression equation. The calibration curve of Doxorubicin was prepared by making different concentrations of the drug in distilled water in a duplicate manner and then recorded their absorbance.

3.2.5 Characterization of Nanoparticles

The size and morphology of the nanoparticles formed were analyzed using field emission scanning electron microscopy (FE-SEM). The sample of iron oxide, gold-coated iron oxide, and chitosan loaded with Doxorubicin with gold-coated iron oxide nanoparticles was prepared and then the SEM image was taken. The elemental composition of nanoparticles was confirmed by the Energy Dispersive X-ray spectroscopy (EDX). Similarly, it also confirms gold-coating on magnetic nanoparticles and the presence of gold-coated iron oxide nanoparticles in chitosan.

X-ray diffraction (XRD) was also used for the characterization of nanoparticles which provides information regarding the crystal structure. The sample was taken in powdered form. The composition of particles was confirmed by comparing the position and intensity of the peaks with the standard available data.

3.2.6 Encapsulation efficiency

It is the percentage of the amount of drug loaded inside the nanoparticles as compared to the amount of drug loaded. So, there are two different ways to calculate the encapsulation efficiency – The direct method and the Indirect method.

1. Direct method- In this method, the pellet was broken by acetic acid, and then reading was taken using a UV-vis spectrophotometer and then compared with the calibration curve of Doxorubicin using $y = mx + c$

   Direct method EE (%) = (A_1 / A_0) X 100

2. Indirect method- In this method, the supernatant we stored after centrifugation was used. The reading was taken and then subtracted from the initial concentration of the drug taken.

Indirect method EE (%) = $(A_0 - A_2/ A_0) X 100$

Where $\mathbf{A_0}$ = amount of drug initially taken, $\mathbf{A_1}$ = amount of drug loaded, and $\mathbf{A_2}$ = amount of drug present in the supernatant

3.2.7 *In vitro* drug release

In vitro, drug release is a study used to find out how much of the drug is released from the nanoparticles at different time intervals. This was done with the help of a dialysis membrane and 80 ml of PBS buffer with a pH of 7.4. The drug-loaded nanohybrids were suspended with 3 ml of PBS and added into a dialysis bag each having 1 ml of resuspended nanohybrids and kept on a magnetic stirrer at 200 rpm and 37° C. Then 1 ml of sample was withdrawn at different time intervals by replacing with 1 ml of fresh PBS. The readings of the withdrawn samples were taken using a UV-Vis spectrophotometer at 480 nm for 10 days, then the percentage of drug release was calculated.

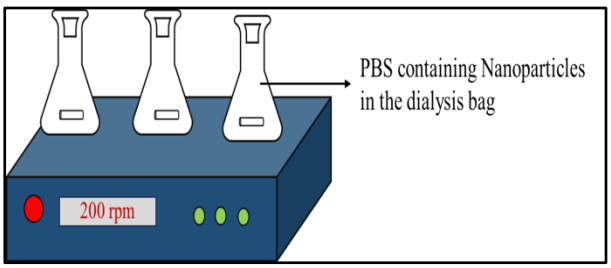

Figure 3.3: *In vitro* drug release from Dox-loaded nanoparticles without exposure to 0.67 W, 808 nm NIR laser

3.2.8 Laser-induced drug release

The pellet of nanohybrids was resuspended with 2 ml of PBS in MCT and given exposure to NIR laser (0.67 W, 808 nm) for 10 mins. After exposure, the temperature was recorded and centrifuged for 10 mins. After the completion of the centrifuge, the supernatant was collected and the absorbance was measured using a UV- Vis spectrophotometer. This was repeated 4 times to calculate the rise in temperature and drug released by the NIR laser with power density 9.49 W/cm^2 (0.67 W, 808 nm).

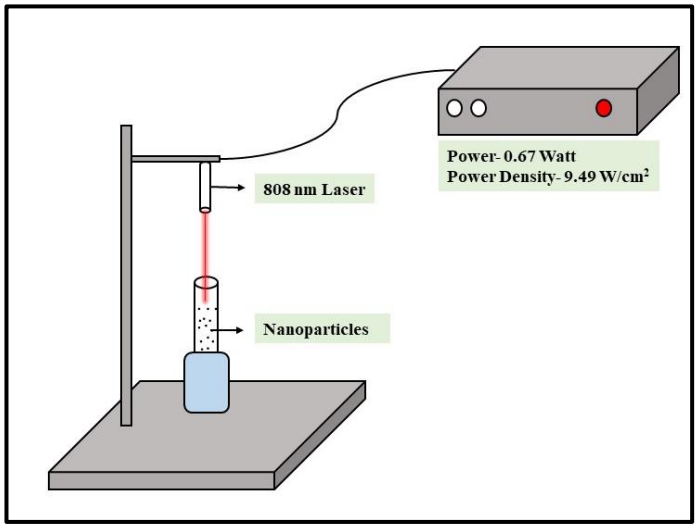

Figure 3.4: *In vitro* drug release from Dox-loaded nanoparticles after exposure with 0.67 W, 808 nm NIR laser for 10 minutes (4 pulses)

3.2.9 Infrared imaging using an IR thermal camera

The rise in temperature due to NIR laser (0.67 W, 808 nm) exposure on nanohybrids (10 min) was checked with an IR thermal camera. The sample of nanoparticles was prepared with different concentrations. With a range of 0%, 10%, 30%, 50%, 70%, and 100%, and were exposed to a 0.67 W, 808 nm NIR laser for 10 minutes. The change in temperature was

visualized by a thermogram generated by an IR thermal camera (Fluke PT i120).

3.2.10 In vitro study of cytotoxicity

The cytotoxicity of the synthesized nanohybrids was calculated by performing an MTT assay. The healthy kidney cells (HEK 293) and breast cancer cells (MCF-7) were seeded in a 96-well plate (7000 cells in each well) allowing them to gain confluency, the cells were further treated with the nanohybrids and incubated for 48 hrs. After incubation, 200 µl of MTT solution was added to each well followed by incubation of 3 hours for the reduction of soluble yellow MTT to insoluble purple formazan crystal inside the cells. Then 100 µl DMSO was added to dissolve these crystals and the absorbance was measured at 570 nm by a microplate reader. The relative or percentage cell viability was calculated by normalizing the absorbance with control. The biocompatibility of synthesized nanohybrids and the cytotoxicity of the drug-loaded nanohybrids were checked on both HEK 293 and MCF-7 cell lines. The IC_{50} value was calculated.

3.2.11 Cellular uptake of Dox-loaded nanohybrid

The uptake of Dox-loaded nanohybrids were evaluated in MCF-7 cells. 15,000 cells per well seeded in confocal wells and allowed to grow in DMEM media with 10 % FBS and 1 % antibiotic till the confluency is achieved. After 24 hours, the cells were treated with Dox-loaded nanohybrids for 6 hrs. After incubation, the media was removed and the cells were washed with PBS to remove the unbound nanoparticles and then the cells were visualized under a confocal microscope at 20X.

3.2.12 Live and Dead Analysis by MTT

The population of cells killed by being treated with drug-loaded nanohybrids followed by laser eradication was studied by performing the live dead assay. 10,000 cells per well were seeded in 96 well plates and allowed to grow in DMEM media with 10% FBS and 1% antibiotic. The cells were treated with nanocarriers and drug-loaded nanohybrids at two different concentrations and incubated for 6 hrs. After incubation, the cells were exposed to 4 pulses of 0.67 W, 808 nm NIR laser for 10 mins and again incubated for 2 hours. A similar experiment was done in which the cells were treated with nanocarriers and drug-loaded nanohybrids without 0.67 W, 808 nm NIR laser exposure. Then 100 µl of MTT solution was added in each well and left for 3 hours for the reduction of soluble tetrazolium crystals to insoluble formazan crystals. Then MTT was removed 100 µl DMSO was added and absorbance was taken at 570 nm and 590 nm using a microplate reader and the percentage of cell viability was calculated by normalizing the absorbance with control.

In another 96-well plate, again the MTT was done in which different concentrations of nanocarriers were added to check the photothermal effect of nanoparticles.

3.2.13 Live and Dead Assay by CLSM

The Live and Dead assay was done to check the number of cells live and dead after treating MCF-7 with nanohybrids. The 10,000 MCF-7 cells per well were seeded in confocal wells and allowed to grow in complete DMEM media. Then the cells were treated with different concentrations of nanohybrids and drug-loaded nanohybrids and incubated for different intervals according to the desired experiment. For the staining of live cells, Glycylphenyl-aminofluorocoumarin (GF-AFC) dye and for dead cells Propidium iodide (PI) dye were used.

The spent medium containing the dead cells was collected in MCTs from the respective wells and centrifuged at 400 g-500 g for 5 mins. Meanwhile, for the staining of live cells, the GF-AFC stock was added to the assay buffer at 1/1000 dilution and supplemented to the cells. After the centrifugation of dead cells, the supernatant was removed gently, and 10 µg/ml of PI dye was added. Both the cell populations were mixed and allowed to incubate for 20 minutes in the dark. Then the fluorescent cells were visualized by confocal microscope by exciting the GF-AFC and PI dye at 405 nm and 588 nm.

3.2.14 Cytotracker staining

The change in integrity of cytoplasm due to photothermal therapy was analyzed by staining with cytotracker dye. 15000 cells/ well were seeded in a confocal well. After treatment with nanocarriers and drug-loaded nanohybrids for 6hrs followed by exposure with 4 pulses of NIR laser (0.67 W, 808 nm) for 10mins each the cells were treated with cytotracker dye and visualized under confocal laser microscopy in 40X magnification.

3.2.15 Live and Dead assay on Spheroids

The effect of the response of laser with the nanocarriers and drug-loaded nanohybrids with the 3D spheroids was analyzed. Approximately 5000 MCF-7 breast cancer cells were allowed to grow in a 3D manner to form a 3D spheroid. After the formation of a complete spheroid, they were treated with nanocarriers only and drug-loaded nanohybrids. After incubation of 6 hrs, the treated spheroids were similarly exposed to NIR laser (0.67 W, 808 nm) like 2D cells. Later the spheroids were treated with Calcein dye and PI dye for live and dead cell analysis and were visualized under a confocal laser microscope with 10X magnification.

Chapter 4

Result and discussion

4.1 Characterization of Iron oxide nanoparticles

4.1.1 Absorbance spectra of Iron oxide nanoparticles

When the absorbance of synthesized iron oxide nanoparticles was taken using a UV Vis spectrophotometer, a broad spectrum was obtained from 300 nm to 900 nm which is used for photothermal therapy with a λ_{max} at 392 nm.

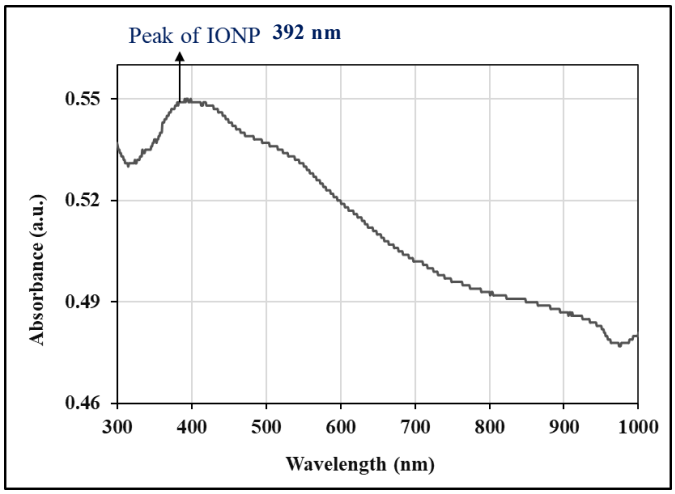

Figure 4.1: Absorbance graph of iron oxide nanoparticles which shows maximum absorbance at 392 nm

4.1.2 Morphological analysis

The size and shape of iron oxide nanoparticles were analyzed by FESEM. The iron oxide was spherical and uniform in size and shape as can be seen in Figure 4.2. The size of magnetic particles was calculated and found to be 23 ± 7 nm.

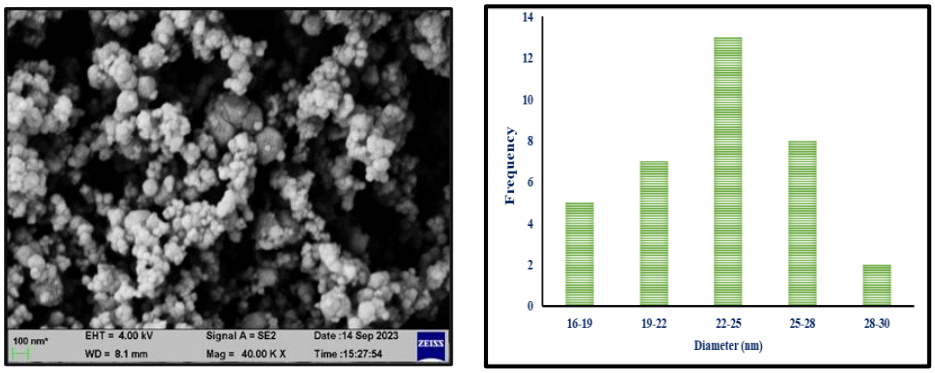

Figure 4.2: SEM image of iron oxide nanoparticles with particle size distribution curve with an average size of 23 ± 7 nm

The magnetic properties of iron oxide nanoparticles were observed. When a magnetic bar was placed near them the nanoparticles were attracted and formed a cluster as seen in Figure 4.3.

Figure 4.3: Magnetic nanoparticles getting attracted toward a magnetic bar

4.2 Characterization of gold-coated iron oxide nanoparticles

4.2.1 Absorbance spectra of gold-coated iron oxide nanoparticles

The absorbance graph of gold-coated iron oxide nanoparticles was taken using a UV- Vis spectrophotometer which shows two different peaks, one at 392 nm which was a characteristic peak of iron oxide nanoparticles,

and another peak at 530 nm which was a characteristic peak of gold. From this graph, we can say that the gold coating may be present on iron oxide nanoparticles.

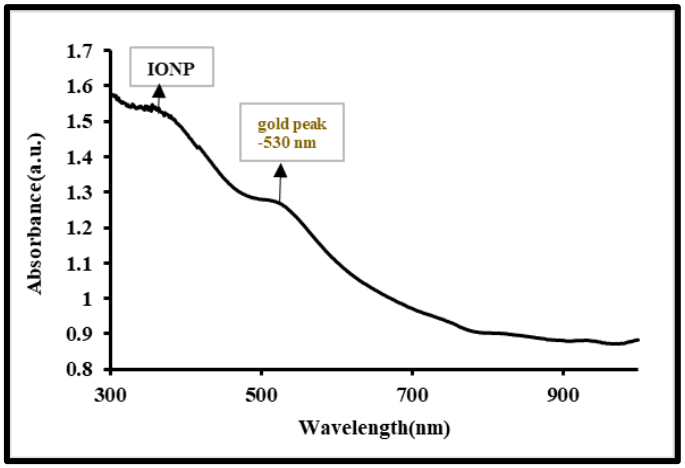

Figure 4.4: Absorbance graph of gold-coated iron oxide nanoparticles showing peak at 392 nm and 530 nm

4.2.2 Morphological analysis

The size and shape of gold-coated iron oxide nanoparticles were observed by FESEM. The gold-coated iron oxide nanoparticles were spherical and uniform in size as seen in figure 4.5. The average size of the gold-coated nanoparticles was found to be 27 ± 9 nm.

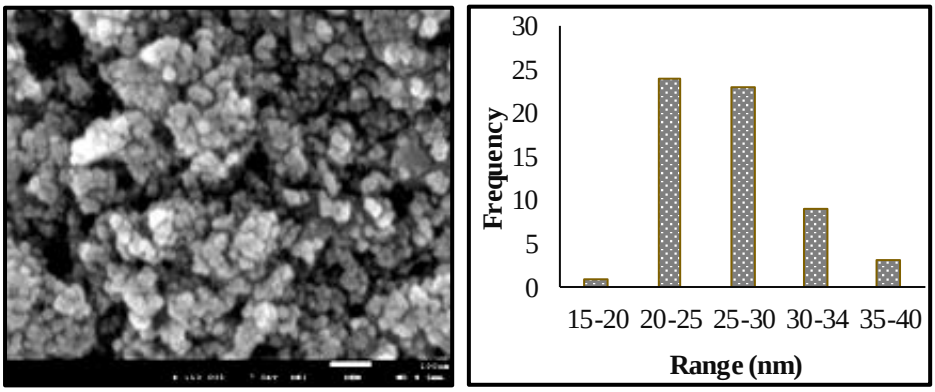

Figure 4.5: SEM image of gold-coated iron oxide nanoparticles with particle-sized distribution curve with an average size of 27 ± 9 nm

4.2.3 Confirmation of Elemental Composition

The EDX was done to confirm the elemental composition of nanoparticles. As per EDX data, the percentage of iron was 16.05% and the gold-coating present on iron oxide nanoparticles was found to be 7.77%. The oxygen was also present in 55.30%.

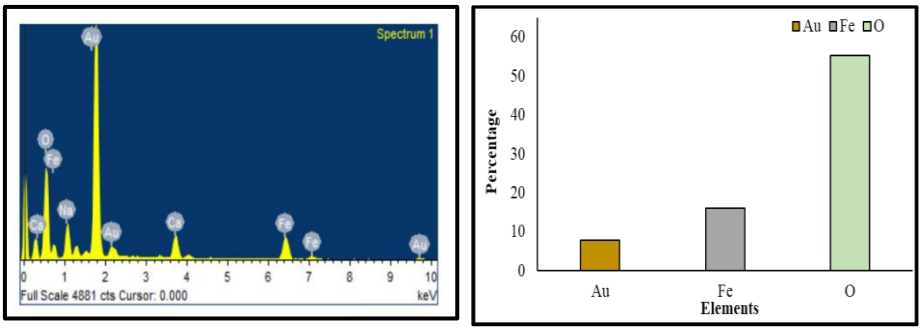

Figure 4.6: EDX analysis of gold-coated iron oxide nanoparticles showing that weight % of gold is 7.77 and iron is 16.05%

4.2.4 XRD analysis

The below figure represents the XRD spectra of gold-coated iron oxide nanoparticles which demonstrates the crystalline structure of the particles. The formation of gold-coated nanoparticles was confirmed by matching the peaks with reference. The different peaks obtained for magnetic nanoparticles at 2θ values are 30.3° (220), 35.6° (311), 43.2° (400), 53.4° (422), and 57.2° (511) whereas, 2θ values for gold are 38.2° (111) and 44.4° (200). So, the pattern of both gold and magnetic oxide peaks matches with the reference and confirms the gold-coating of iron oxide nanoparticles.

The peak of our synthesized nanoparticles was also compared with the reported peak of α-Fe_2O_3 and γ-Fe_2O_3 for conformation of the formation

of Fe_3O_4. Additional peaks of α-Fe_2O_3 were reported at 210° and 213° whereas in the case of γ-Fe_2O_3 was present at 31°. These peaks were absent in the XRD spectra of our synthesized nanoparticles. This confirms that the synthesized nanoparticles were Fe_3O_4 (Das et al., 2020).

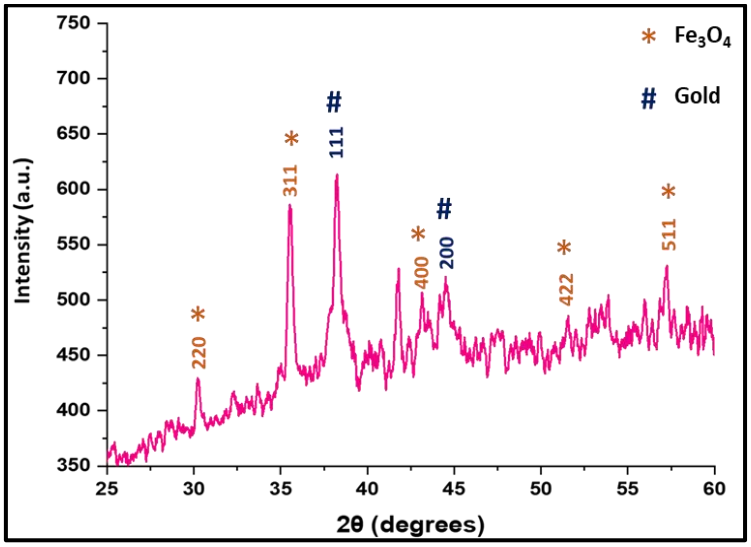

Figure 4.7: XRD analysis of gold-coated iron oxide nanoparticles

4.3 Characterization of chitosan loaded with Doxorubicin with gold-coated iron oxide nanoparticles

4.3.1 Absorbance spectra of chitosan loaded with Doxorubicin with gold-coated iron oxide nanoparticles

The absorbance of nanohybrid was taken using UV-vis spectrophotometer and two different peaks were observed, first at 480 nm which was a characteristic peak of the Doxorubicin, and the second at 530 nm which was a peak of gold. This implies that the drug was encapsulated in chitosan and gold-coated iron oxide nanoparticles were also present in the nanohybrid. For confirmation of gold coating on iron oxide nanoparticles, further analysis was done.

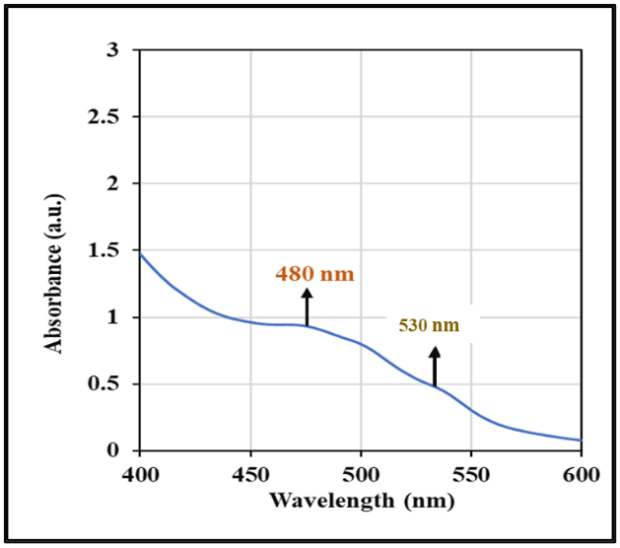

Figure 4.8: Absorbance graph of chitosan loaded with dox with gold-coated iron oxide nanoparticles showing peaks at 480 nm and 530 nm

4.3.2 Morphological analysis

The morphology and size of chitosan loaded with Doxorubicin with gold-coated iron oxide were confirmed by FESEM. The shape of nanoparticles were found to be spherical in shape having an average size of approximately 115 ± 15 nm.

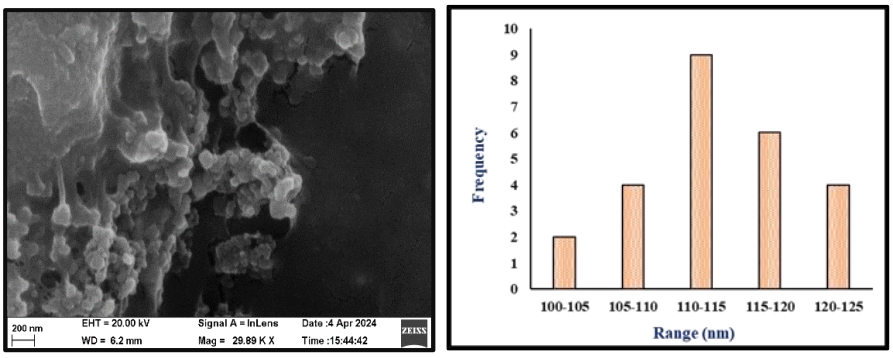

Figure 4.9: SEM image of chitosan loaded with Dox with gold-coated iron oxide nanoparticles with particle size distribution curve with an average size of 115 ± 15 nm

4.3.3 Confirmation of elemental composition by EDX analysis

The EDX was done to confirm the elemental composition of nanoparticles. According to EDX analysis, the percentage of iron present was 9.12 % and gold was 3.4 weight %. The carbon and oxygen were also present in 28 and 49.12 weight %.

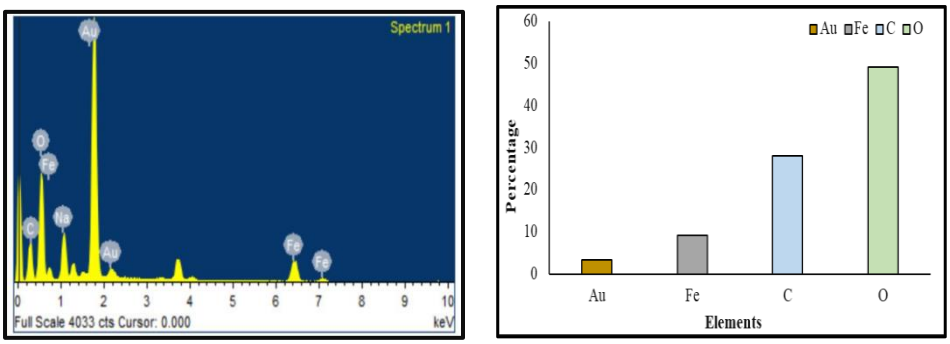

Figure 4.10: EDX analysis of Chitosan loaded with Dox with gold-coated iron oxide nanoparticles which shows that 9.12 weight % of iron and 3.4 weight % of gold were present

4.3.4 XRD analysis of nanohybrids

The below figure represents the XRD spectra of gold-coated iron oxide nanoparticles which demonstrates the crystalline structure of the particles. The formation of gold-coated nanoparticles was confirmed by matching the peaks with reference. Two different peaks were obtained at 43.2° (400) and 44.4° (200) which is a characteristic peak of iron oxide nanoparticles and gold. This confirms the formation of gold-coated iron oxide nanoparticles with chitosan.

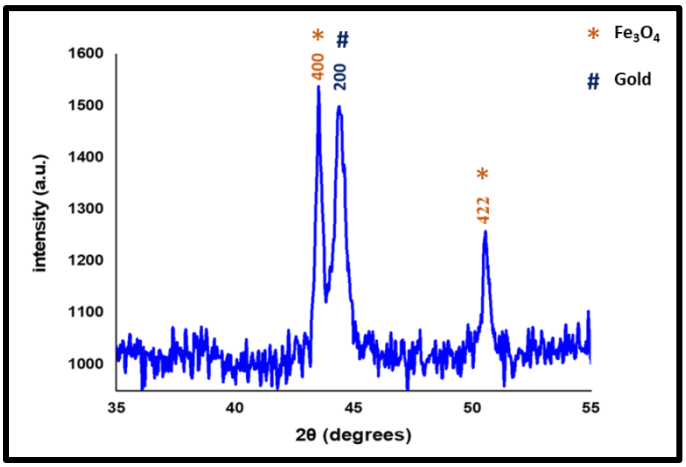

Figure 4.11: XRD spectra of chitosan loaded with Dox with gold-coated iron oxide nanoparticles

4.4 The calibration curve of Doxorubicin

The UV-visible spectrophotometer was used to find out the absorbance which works on the principle of Beer's Lambert law which states that the absorbance and concentration are directly proportional to each other. Using a UV-visible spectrophotometer we had taken a spectrum of Doxorubicin drugs to check their specific absorbance peak. The specific absorbance of the Doxorubicin drug is at 480 nm.

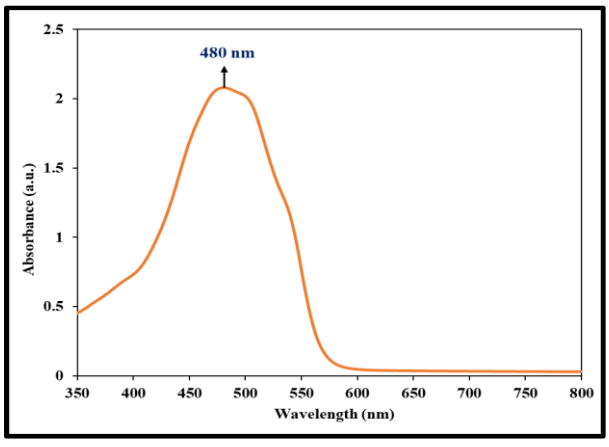

Figure 4.12: Absorbance graph of Dox which shows maximum absorbance at 480 nm

The calibration curve of Doxorubicin was plotted in which different concentrations of the drug were made in distilled water and absorbance was taken. The R^2 value and equation will be used to find the encapsulation efficiency and other calculations. The obtained regression equation was $y = 0.0171x + 0.037$ and the linearity coefficient (R^2) value was 0.996 which was near 1.

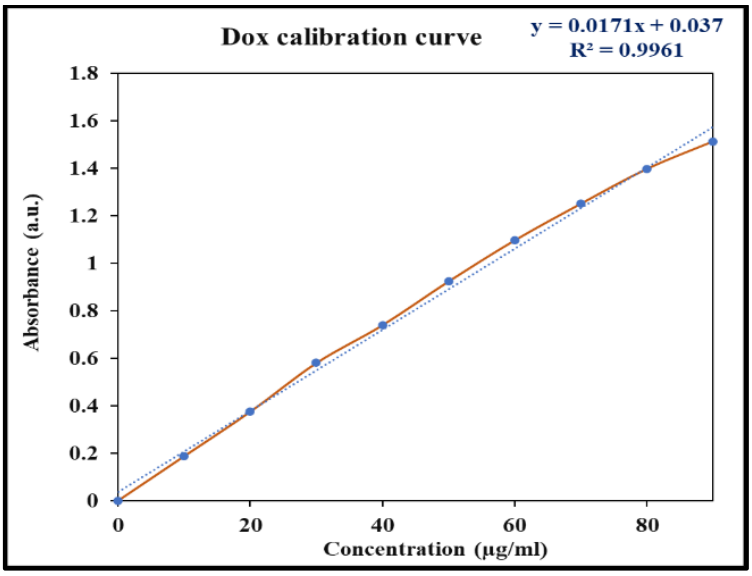

Figure 4.13: Calibration curve of Dox at 480 nm with R^2 value of 0.996

4.5 Encapsulation efficiency

The encapsulation efficiency of synthesized nanohybrid was calculated to find the amount of drug encapsulated inside the synthesized nanoparticles as compared to the amount of drug initially taken. It is calculated by using two different methods with the help of the calibration curve we obtained. In the indirect method, the reading of the supernatant was subtracted from an initial concentration of the drug taken initially whereas in the direct method, the reading of the pellet broken by acetic acid was taken.

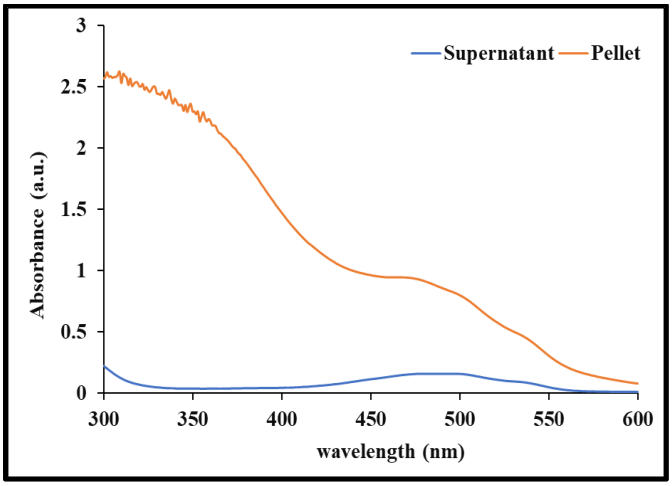

Figure 4.14: Absorbance of supernatant and Dox-loaded nanohybrid broken by acetic acid for calculation of EE (%)

The encapsulation efficiency of the drug by indirect method was 78.82 ± 6 %. Whereas, the encapsulation efficiency of the drug by direct method was calculated by breaking the pellet of nanoparticles with 1% acetic acid and calculated as 82.37 ± 7 %.

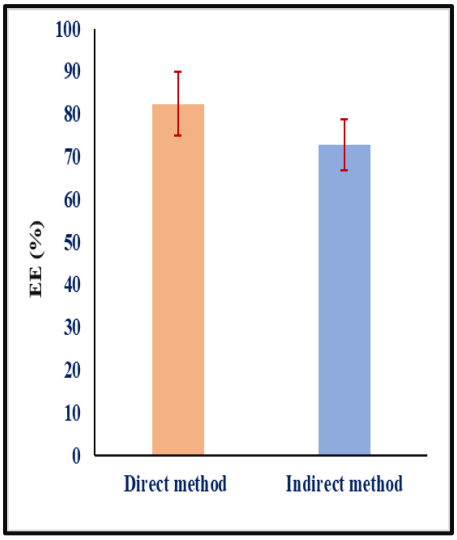

Figure 4.15: Graph showing EE % of Dox by the direct method was 78.8 % and by the indirect method was 82.3 %

4.6 *In vitro* drug release without laser

The release of the drug from nanoparticles was done using the dialysis bag and PBS buffer of pH 7.4 for 10 days in triplicates. There was an initial burst out of the drug was found in the initial 12 hours and then it was the very sustained release of the drug leading to the almost equilibrium stage.

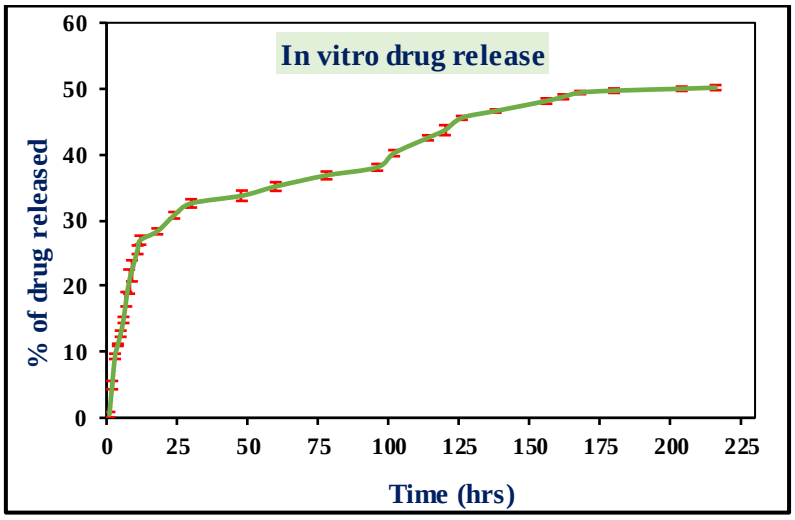

Figure 4.16: *In vitro* drug release without exposure to laser at pH 7.4

4.7 Laser-induced drug release

The pellet of Dox-loaded nanohybrids was resuspended in 2 ml PBS and 10 min of NIR laser (0.67 W, 808 nm) was given. The four pulses of laser were given to the sample and then the temperature rise and the percentage of drugs released were recorded after every pulse of laser. 17.7 % of the drug was released from nanohybrids after 4 pulses of NIR laser. After 1st pulse of the laser for 10 minutes 14° C rise in temperature was seen and then more than a 15° C rise in temperature was seen.

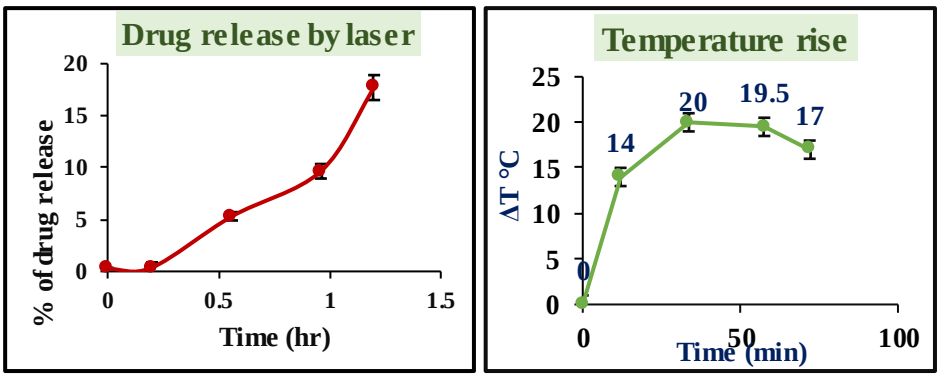

Figure 4.17: *In vitro* drug release on exposing drug-loaded nanohybrids with 0.67 W, 808 nm NIR laser with rise in temperature

4.8 IR thermal imaging

Thermal imaging was done to analyse the heat emitted from various objects. The thermal energy released from the object is in the form of infrared (IR), is captured by a thermal imaging camera and displayed in the form of a thermogram which is the visual output produced by the thermal camera having different colors of the visible range (400 to 700 nm) representing different temperatures. The hotter or high-temperature areas are represented by red color whereas cooler or low-temperature areas are represented by blue color. This is how a thermal camera is used for the detection of temperature.

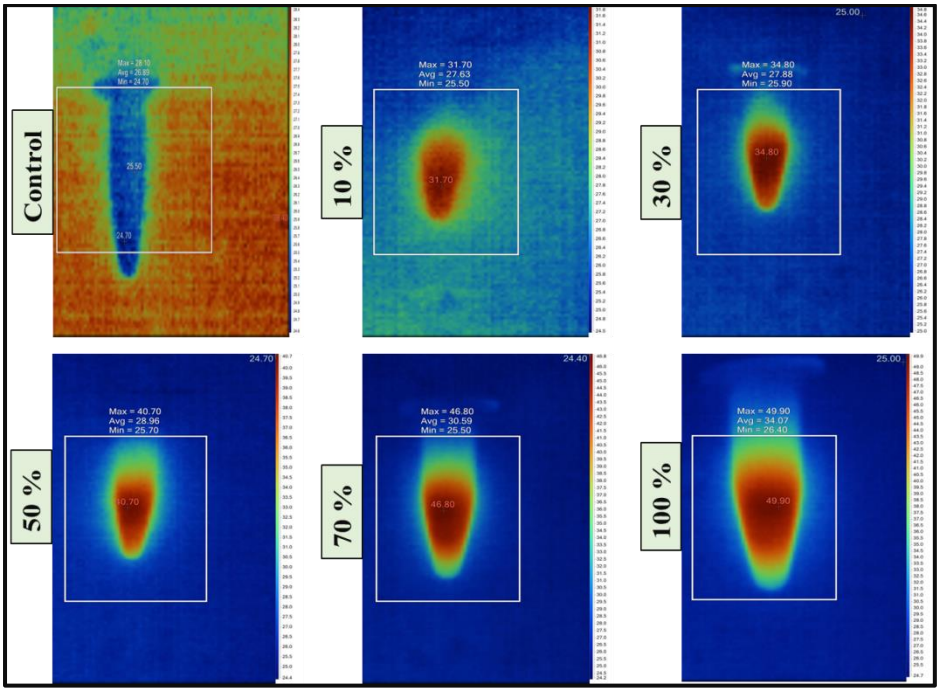

Figure 4.18: Thermal image of different concentrations of nanohybrid after exposure to NIR 0.67 W, 808 nm laser for 10 minutes by using IR thermal imaging camera

After exposing different concentrations of nanohybrid with NIR 0.67 W, 808 nm laser the temperature of the surrounding rises which was recorded with the help of a thermal camera as shown in figure 4.18. From the above figure, we can analyze that increasing concentration of nanohybrids is directly proportional to temperature rise. The maximum temperature recorded was 49.90º C at 100 % concentration with respect to control. This shows that the when the synthesized nanohybrid was exposed to 0.67 W, 808 nm laser for 10 minutes the temperature of the surroundings increased showing the property of photothermal effect.

4.9 In Vitro cell toxicity by MTT analysis

The cytotoxicity effect of nanohybrid was calculated by performing a colorimetric MTT assay. This assay is based on cell viability of the cells

in which the soluble yellow MTT (3-(4,5-dimethylthiazol-2-yl)-2,5-diphenyltetrazolium bromide) is reduced to insoluble purple formazan crystal by NADPH dependent oxidoreductase enzyme. Then, these insoluble crystals are dissolved by using DMSO, and the resulting coloured solution is quantified by taking absorbance at 570 nm and 590 nm using a spectrophotometer.

At low concentrations, the nanocarriers were not toxic for both MCF-7 and HEK 293 cells and as the concentration of nanocarriers increased a decrease in cell viability was seen.

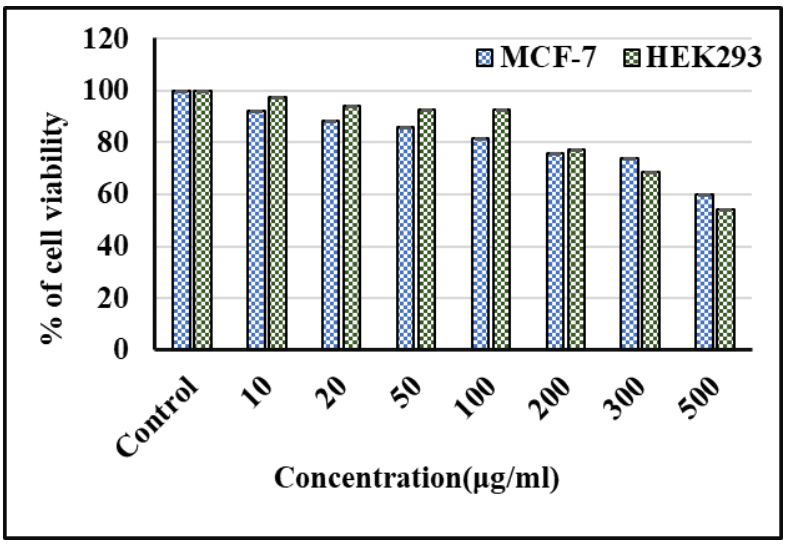

Figure 4.19: The cell viability assay on treating MCF-7 and HEK 293 with nanocarriers

Similarly, the cytotoxicity effect of drug-loaded nanohybrid was calculated by performing an MTT assay on HEK 293 and MCF-7 cells. At low concentrations, the nanocarriers were not toxic for both MCF-7 and HEK 293 cells. The IC_{50} value of drug-loaded nanohybrids on HEK 293 was found to be 1.54 µg/ml whereas IC_{50} value on MCF-7 was 1.04 µg/ml.

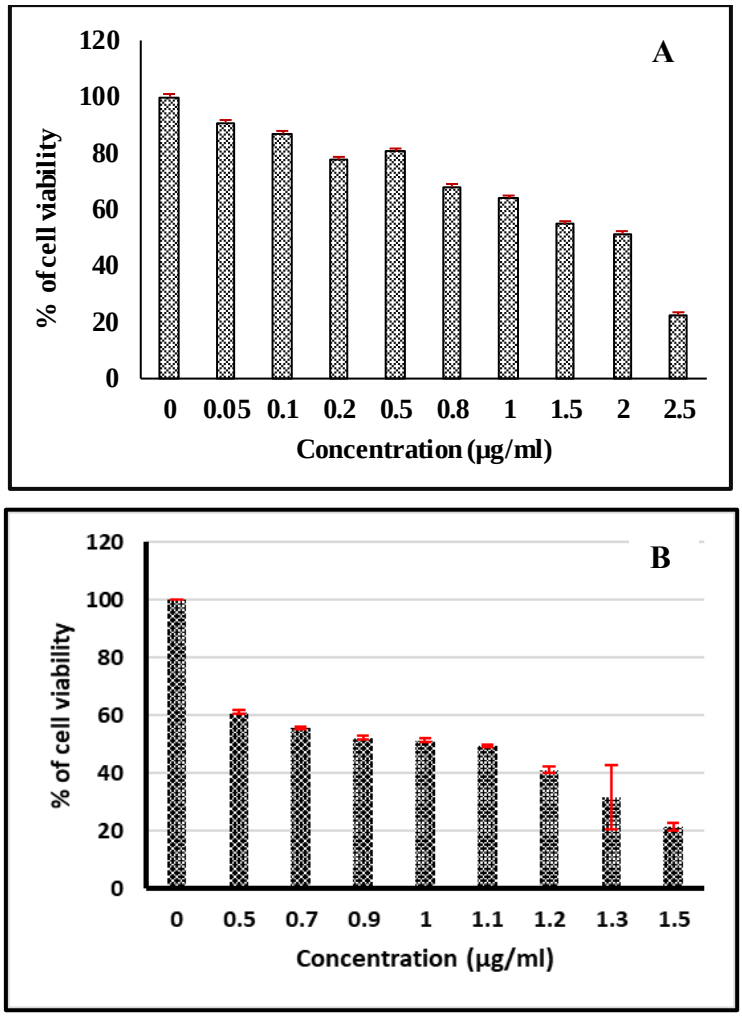

Figure 4. 20: The percentage of cell viability of drug-loaded nanohybrids on HEK 293 (**A**) with IC_{50} value of 1.54 µg/ml and on MCF-7 (**B**) with an IC_{50} value of 1.04 µg/ml

4.10 Cellular uptake of Dox-loaded nanohybrid

The cellular uptake of Dox-loaded nanohybrid was investigated with the MCF-7 breast cancer cell line. Doxorubicin is an auto fluorescence compound which emits green fluorescence signal at 525 nm. After incubating MCF-7 with Dox-loaded nanohybrids for 6 hours, intensity of green signal was observed as compared to control as shown in figure 4.21.

This shows that Dox-loaded nanoparticles got internalized in MCF-7 within 6 hrs.

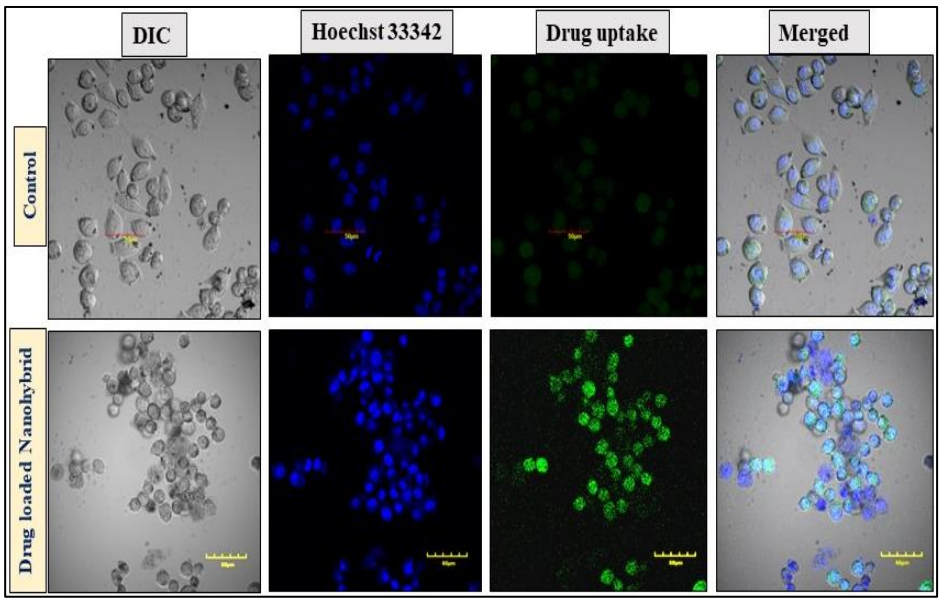

Figure 4.21: CLSM image of cellular uptake of Dox-loaded nanoparticles in MCF-7 cells

4.11 Photothermal effect on MCF-7 by MTT

The effect of laser with nanocarriers and drug-loaded nanohybrids on MCF-7 with and without exposure of 0.67 W, 808 nm NIR laser was analyzed by performing MTT assay. The MCF-7 cells were seeded and treated with 10 % nanocarriers and drug-loaded nanohybrids at concentrations of 5 µg/ml, 7 µg/ml, and 9 µg/ml. The cells treated with 10 % nanocarriers followed by laser exposure resulted in 60 % cell viability whereas, more cell death was encountered in MCF-7 cells treated with drug-loaded nanohybrids followed by the exposure of NIR laser due to the laser-responsive drug release as well as photothermal effect.

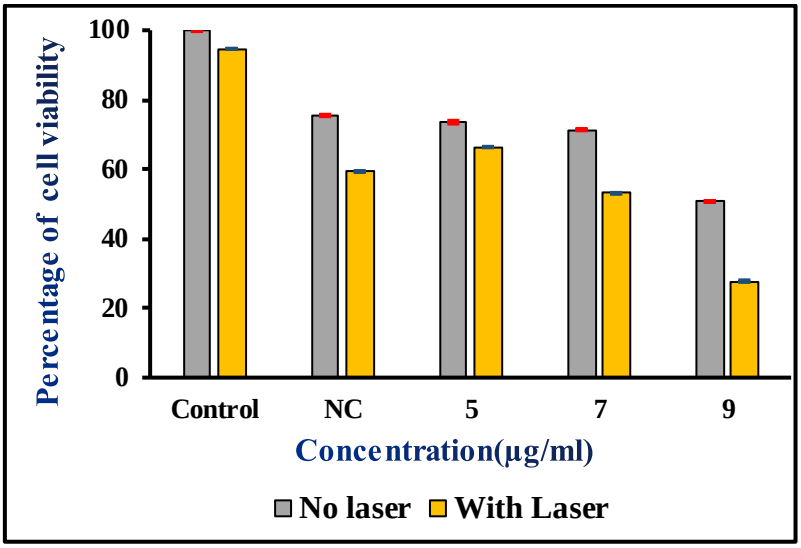

Figure 4.22: The cell viability assay on MCF-7 cells treated with 10 % nanocarriers and 5 µg/ml, 7 µg/ml, and 9 µg/ml drug-loaded nanohybrids

The photothermal efficiency of the nanocarriers on MCF-7 cells treated with different concentrations of nanocarriers followed by exposure to 808 nm NIR laser for 10 minutes (4 pulses) was studied by MTT assay. The percentage of cell viability decreases by increasing the concentration of nanocarriers. The IC_{50} value was obtained at 55 % (v/v) concentration of nanocarriers which This was confirmed the photothermal efficacy of the synthesized nanocarriers.

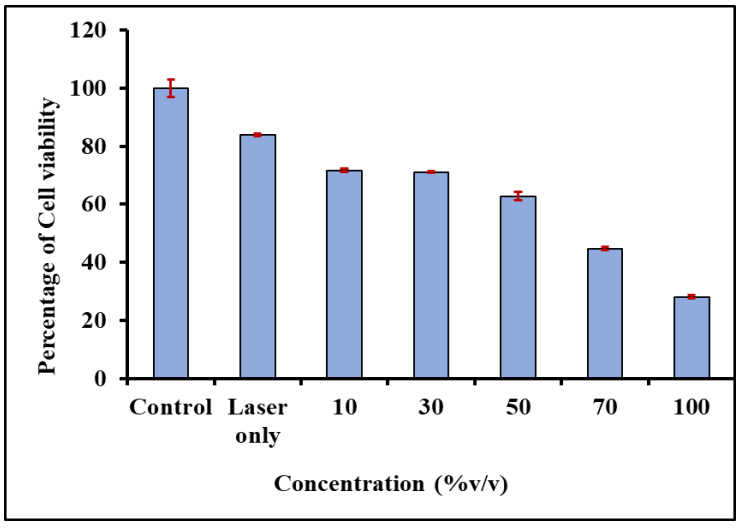

Figure 4.23: The cell viability assay on MCF-7 cells treated with different concentrations of nanocarriers followed by exposure of 0.67 W, 808 nm NIR laser for 10 mins (4 pulses) showing a decrease in cell viability with an IC_{50} of 55 %

4.12 Live and Dead Analysis using CLSM

To ensure the live and dead cells after treatment with nanohybrids followed by laser exposure the cells were stained with GFAFC and Propidium iodide dye (PI). For the staining of live cells, glycylphenylalanyl-aminoflurocoumarin (GF-AFC) was used whereas for the staining of dead cells, PI dye was used. The GF-AFC dye penetrates the cells which act as a substrate for the aminopeptidase enzyme of the cell. The enzyme removes the glycine and phenylamino acid and releases AFC which generates a blue fluorescent signal proportional to living cells. Whereas PI dye-stained dead cells with red colour. It cannot pass through intact cell membranes but freely enters into the compromised cell and intercalates into dsDNA and emits fluorescence. MCF-7 cells were treated with 30 µl of nanocarriers followed by incubation for 2 hours, 4 hours, and 6 hours and then exposed with 4 pulses of 0.67 W, 808 nm NIR laser for 10 minutes. The maximum cell death was seen in cells incubated with nanocarriers for 6 hours (75 %) because there is maximum uptake of nanocarriers in cells. Whereas, in 2-hour and 4-hour incubation with nanocarriers 30 % and 58 % cell death was seen. This shows that the synthesized nanoparticles have photothermal property therefore when we treated MCF-7 cells with nanocarriers followed by the exposure of 0.67 W, 808 nm NIR laser the cell death occurs.

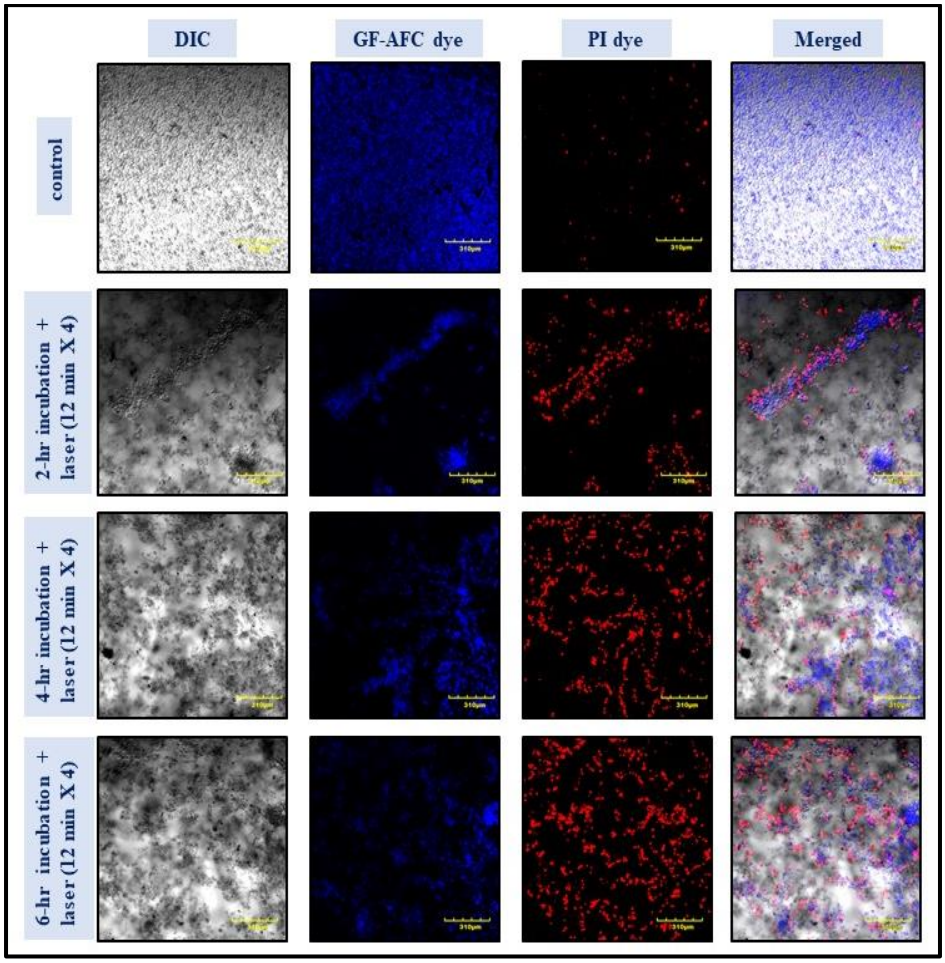

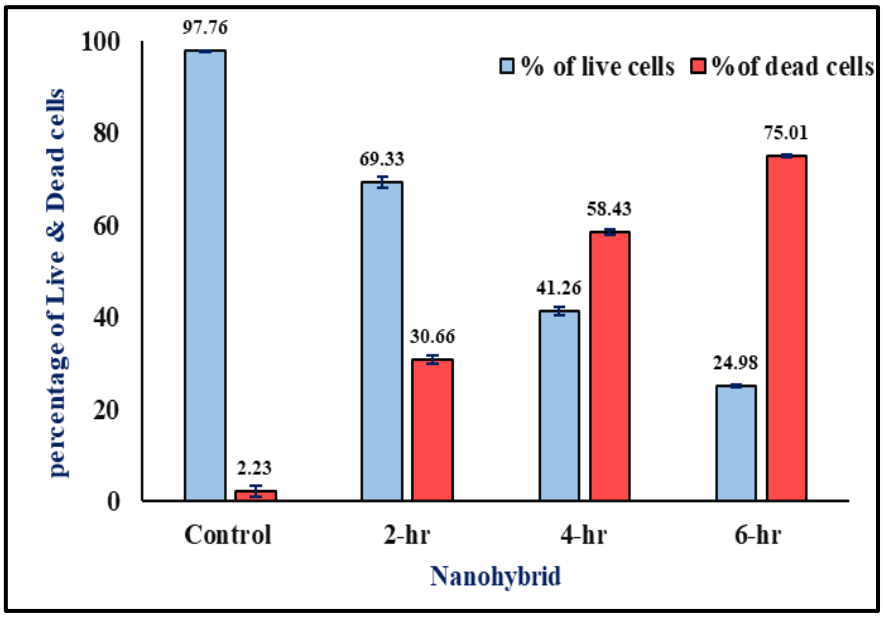

Figure 4.24: Live and Dead analysis- CLSM image of live and dead analysis by confocal microscopy by treating MCF-7 cells with 30 µl of nanocarriers for 2-, 4- and 6-hour incubation followed by exposure of

0.67 W, 808 nm NIR laser with a graphical representation of the percentage of live and dead cells

Next, the MCF-7 cells were treated with 5 µg/ml and 7 µg/ml of drug-loaded nanoparticles and incubated for 6 hours followed by exposure to 0.67 W, 808 nm NIR laser for 10 minutes (4 pulses). When we expose nanoparticles with laser, there is a burst release of drug due to which cell death occurs. The cells treated with drug-loaded nanoparticles show more cell death as compared to the control. In 7 µg/ml, drug-loaded nanohybrid 83% cell death was seen whereas, in 5 µg/ml 74 % cell death was there. This implies that cell death occurs due to the photothermal effect and laser-induced drug release.

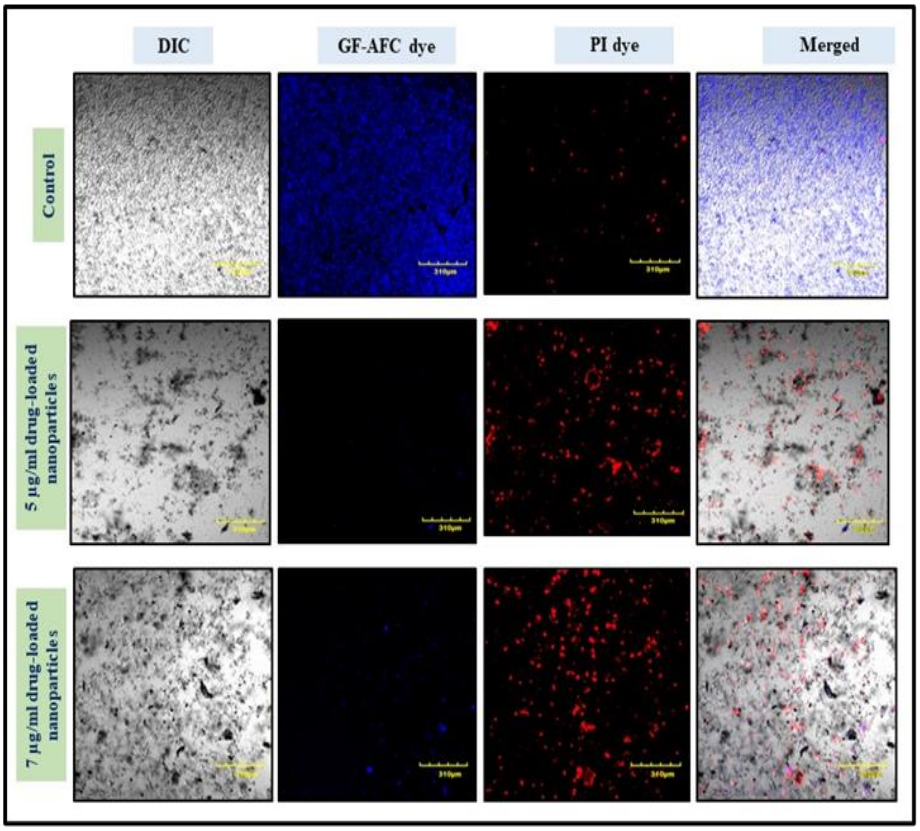

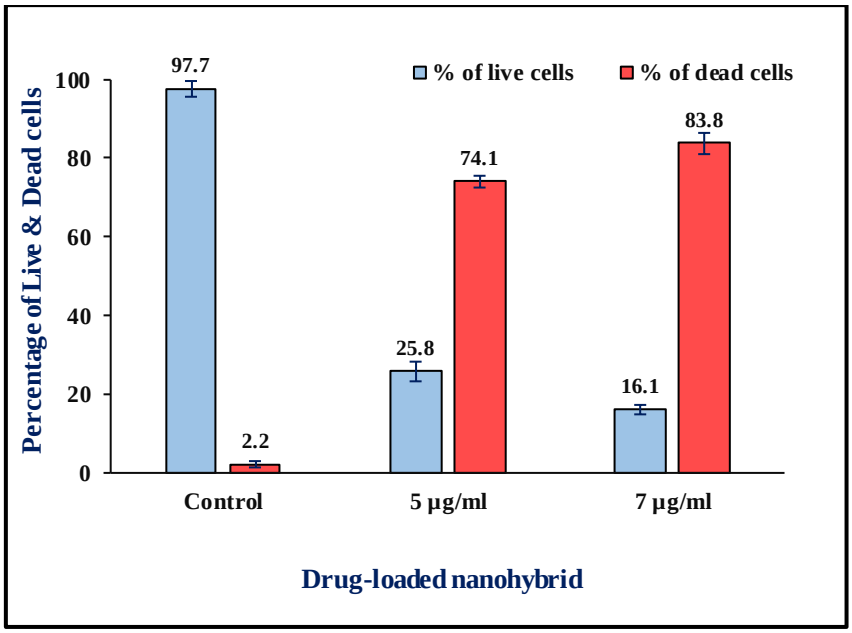

Figure 4.25: Live and Dead analysis using confocal microscopy- CLSM image of live and dead analysis by confocal microscopy by treating MCF-7 cells with 5 µg/ml and 7µg/ml of drug-loaded nanohybrids followed by exposure of 0.67 W, 808 nm NIR laser with a graphical representation of the percentage of live and dead cells.

4.13 Cytotracker

Cytoplasm is the major constituent of our body. The density and integrity of the cytoplasm are responsible for maintaining cellular functions. Due to exposure of laser on synthesized nanocarriers treated cells, the cytoplasm shape and constituent were disturbed. The cytotracker dye was used to check the cytoplasmic volume before and after exposure to the laser. It was seen that the cytoplasm content of nanocarriers treated cells followed by NIR laser (0.67 W, 808 nm) exposure caused a rise in temperature, and due to the photothermal effect, the cytoplasm was burst which caused the death of the cells as shown with a yellow circle. It was also analyzed that the laser exposure on nanocarriers treated cells shows

more damage on cytoplasm in comparison with the cells with only laser exposure.

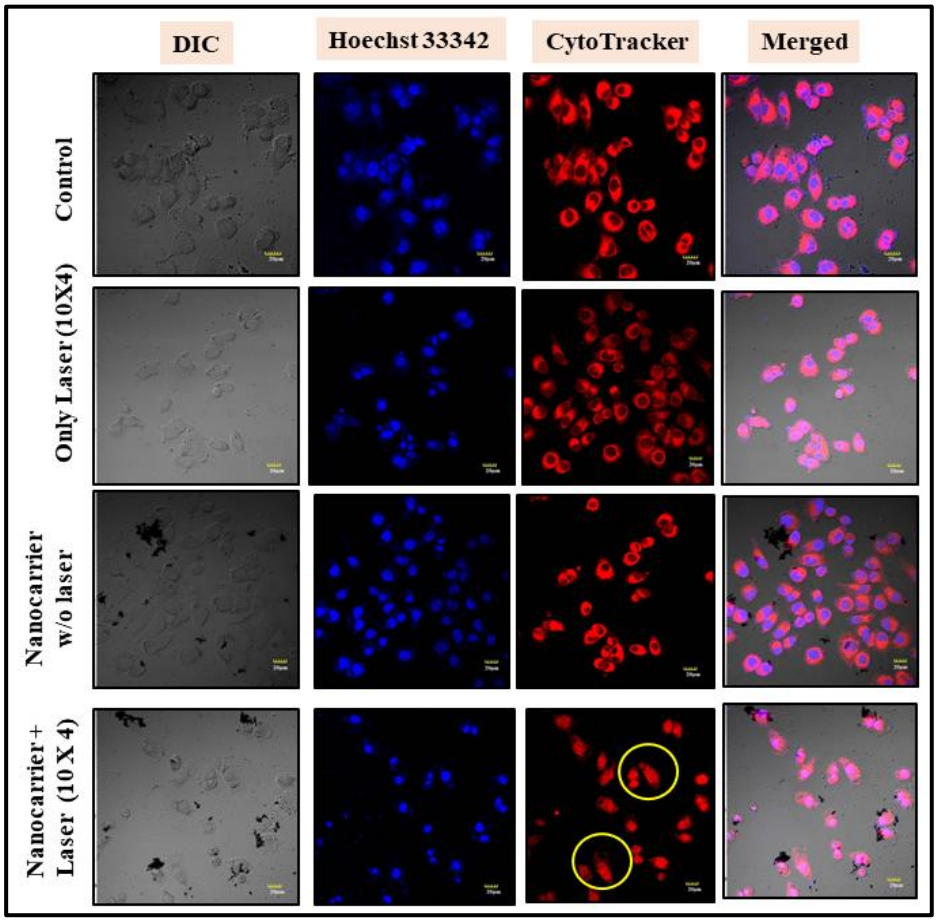

Figure 4.26: Cytotracker- CLSM image of MCF-7 treated with nanocarriers without and with exposure of 808 nm NIR laser for 10 mins (0.67 W, 4 pulses) causes a burst of cytoplasm shown by the yellow circle

4.14 Live and Dead analysis on spheroids

The effect of exposure to laser was analyzed on 3D spheroids after treatment with nanocarriers and drug-loaded nanohybrids by performing live dead assay with calcein and PI dye. After formation, the spheroids were treated with synthesized nanocarriers and Drug-loaded nanohybrids followed by laser exposure. We can visualize that there is more cell death

in the spheroid treated with drug-loaded nanohybrids in comparison with the control and only laser-treated spheroids. Most importantly the integrity of the spheroid was got damaged and the structure was dislocated due to the treatment. In the spheroids treated with only nanocarriers followed by NIR laser exposure also undergo cell damage which may be due to the photothermal effect due to the presence of nanocarriers.

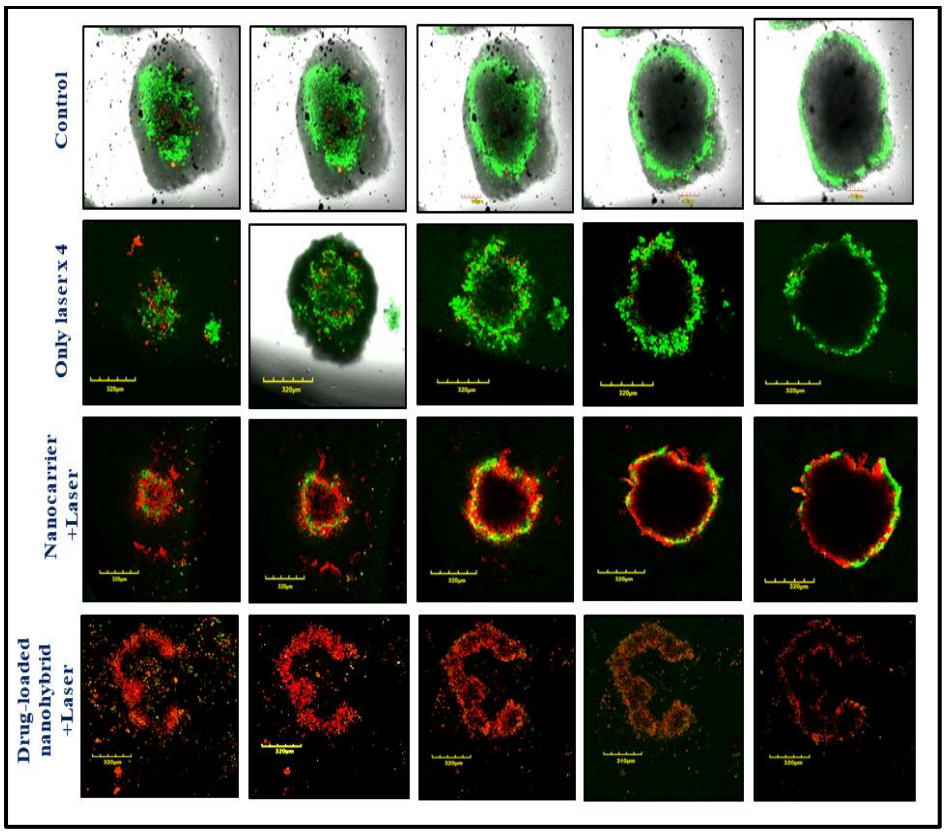

Figure 4.27: Live and Dead assay- CLSM image of the live and dead assay on spheroids by incubating it with nanocarriers and drug-loaded nanohybrids followed by exposure of 0.67 W, 808 nm NIR laser for 10 mins (4 pulses)

Chapter 5

Conclusion

The photothermal therapy is a novel approach for treating cancer. The primary goal is to deliver drugs and release them in a controlled manner. The goal is to kill cancer cells using photothermal therapy. According to literature Iron oxide nanoparticles are widely used for photothermal therapy. It also acts as a contrasting agent in Magnetic Resonance Imaging. However, the disadvantage of using Fe_3O_4 is it degrades into iron ions which generates free radicals leading to cell death (Fu et al., 2020). So, to overcome this gold coating was done on iron oxide nanoparticles due to which it became stable and bio-compatible. For the co-delivery of gold-coated iron oxide nanoparticles along with Doxorubicin chitosan was used as a carrier or vehicle. So, we synthesized a chitosan loaded with Doxorubicin drug with gold-coated iron oxide nanoparticles. These Doxorubicin-loaded chitosan-gold-magnetic nanoparticles offer several advantages. It plays an important role in therapy as well as the diagnosis of cancer by bioimaging. The magnetic nanoparticles were used for photothermal therapy and bioimaging of cancer (Kharey et al., 2023), whereas chitosan, a pH-responsive polymer combined was used for encapsulating both gold-coated magnetic nanoparticles and Doxorubicin and for the sustained release of drugs (Joshi et al., 2020), and gold was used for detecting cancer as well as maintaining the stability of iron oxide nanoparticles.

The synthesized nanoparticles have an average size of 115 nm containing 9.14 weight % of iron and 3.4 weight % of gold. These nanoparticles show 82 % of encapsulation efficiency due to their large size. There was a very sustain and controlled release of drug from the nanohybrids but when the nanohybrids were exposed to 0.67 W, 808 nm NIR laser, a burst release of drug was seen i.e., 18 % drug was released within 1.2 hours.

The temperature rise was seen due to which cell death occurred. The synthesized nanohybrids are bio-compatible in nature.

The drug-loaded nanohybrids got internalized in MCF-7 cells after 6 hours of incubation. From the live and dead analysis of drug-loaded nanohybrids followed by exposure to 0.67 W, 808 nm NIR laser, the percentage of dead cells increases due to the Photothermal effect as well as laser-induced drug release. The live and dead analysis using confocal microscopy was also done on synthesized spheroids of MCF-7 cells. The intensity of live cells decreases successfully and the intensity of dead cells increases on treatment with nanocarriers and drug-loaded nanohybrids followed by exposure to 0.67 W, 808 nm NIR laser for 10 minutes (4 pulses were given).

So, the synthesized nanohybrids are bio-compatible in nature exhibiting the photothermal therapy. In the future, we will use these nanohybrids for bioimaging by MRI and CT scan and also used for *In-vivo* studies.

Chapter 6

References

Curry, T., Epstein, T., Smith, R., & Kopelman, R. (2013). Photothermal therapy of cancer cells mediated by blue hydrogel nanoparticles. *Nanomedicine*, *8*(10), 1577–1586. https://doi.org/10.2217/nnm.12.190

Das, R., Witanachchi, C., Nemati, Z., Kalappattil, V., Rodrigo, I., García, J. Á., Garaio, E., Alonso, J., Lam, V. D., Le, A.-T., Phan, M.-H., & Srikanth, H. (2020). Magnetic Vortex and Hyperthermia Suppression in Multigrain Iron Oxide Nanorings. *Applied Sciences*, *10*(3), 787. https://doi.org/10.3390/app10030787

Estelrich, J., & Busquets, M. A. (2018). Iron Oxide Nanoparticles in Photothermal Therapy. *Molecules*, *23*(7), Article 7. https://doi.org/10.3390/molecules23071567

Fu, S., Man, Y., & Jia, F. (2020). Photothermal Effect of Superparamagnetic Fe_3O_4 Nanoparticles Irradiated by Near-Infrared Laser. *Journal of Nanomaterials*, *2020*, e2832347. https://doi.org/10.1155/2020/2832347

Huang, X., Jain, P. K., El-Sayed, I. H., & El-Sayed, M. A. (2008). Plasmonic photothermal therapy (PPTT) using gold nanoparticles. *Lasers in Medical Science*, *23*(3), 217–228. https://doi.org/10.1007/s10103-007-0470-x

Huang, X., Lu, Y., Guo, M., Du, S., & Han, N. (2021). Recent strategies for nano-based PTT combined with immunotherapy: From a biomaterial point of view. *Theranostics*, *11*(15), 7546–7569. https://doi.org/10.7150/thno.56482

Joshi, B., & Joshi, A. (2022). Polymeric magnetic nanoparticles: A multitargeting approach for brain tumour therapy and imaging. *Drug Delivery and Translational Research*, *12*(7), 1588–1604. https://doi.org/10.1007/s13346-021-01063-9

Joshi, B., Kaur, J., Khan, E., Kumar, A., & Joshi, A. (2020). Ultrasonic atomizer driven development of doxorubicin-chitosan nanoparticles as anticancer therapeutics: Evaluation of anionic cross-linkers. *Journal of Drug Delivery Science and Technology*, *57*, 101618. https://doi.org/10.1016/j.jddst.2020.101618

Joshi, B., Shankar, U., Vishwakarma, S., Kumar, A., Kumar, A., Joshi, D., & Joshi, A. (2023). Multifunctional Ultrasmall Theranostic Nanohybrids

Developed by Ultrasonic Atomizer for Drug Delivery and Magnetic Resonance Imaging. *ACS Applied Bio Materials*, *6*(5), 1943–1952. https://doi.org/10.1021/acsabm.3c00151

Kaur, J., Jakhmola, S., Singh, R. R., Joshi, B., Jha, H. C., & Joshi, A. (2021). Ultrasonic Atomizer-Driven Development of Biocompatible and Biodegradable Poly(d,l-lactide-co-glycolide) Nanocarrier-Encapsulated Suberoylanilide Hydroxamic Acid to Combat Brain Cancer. *ACS Applied Bio Materials*, *4*(7), 5627–5637. https://doi.org/10.1021/acsabm.1c00430

Kharey, P., Goel, M., Husain, Z., Gupta, R., Sharma, D., Manikandan, M., Palani, I. A., & Gupta, S. (2023). Green synthesis of biocompatible superparamagnetic iron oxide-gold composite nanoparticles for magnetic resonance imaging, hyperthermia and photothermal therapeutic applications. *Materials Chemistry and Physics*, *293*, 126859.

Meng, F., Zhong, Y., Cheng, R., Deng, C., & Zhong, Z. (2014). pH-sensitive polymeric nanoparticles for tumor-targeting doxorubicin delivery: Concept and recent advances. *Nanomedicine*, *9*(3), 487–499. https://doi.org/10.2217/nnm.13.212

Mohanraj, V. J., & Chen, Y. (2006). Nanoparticles—A review. *Tropical Journal of Pharmaceutical Research*, *5*(1), Article 1. https://doi.org/10.4314/tjpr.v5i1.14634

Narayanan, S., Sathy, B. N., Mony, U., Koyakutty, M., Nair, S. V., & Menon, D. (2012). Biocompatible Magnetite/Gold Nanohybrid Contrast Agents via Green Chemistry for MRI and CT Bioimaging. *ACS Applied Materials & Interfaces*, *4*(1), 251–260. https://doi.org/10.1021/am201311c

Salem, D. S., Sliem, M. A., El-Sesy, M., Shouman, S. A., & Badr, Y. (2018). Improved chemo-photothermal therapy of hepatocellular carcinoma using chitosan-coated gold nanoparticles. *Journal of Photochemistry and Photobiology B: Biology*, *182*, 92–99. https://doi.org/10.1016/j.jphotobiol.2018.03.024

Shen, C.-L., Liu, H.-R., Lou, Q., Wang, F., Liu, K.-K., Dong, L., & Shan, C.-X. (2022). Recent progress of carbon dots in targeted bioimaging and cancer therapy. *Theranostics*, *12*(6), 2860–2893. https://doi.org/10.7150/thno.70721

Thorn, C. F., Oshiro, C., Marsh, S., Hernandez-Boussard, T., McLeod, H., Klein, T. E., & Altman, R. B. (2011). Doxorubicin pathways: Pharmacodynamics and adverse effects. *Pharmacogenetics and Genomics*, *21*(7), 440–446. https://doi.org/10.1097/FPC.0b013e32833ffb56

Yang, J., Fan, L., Xu, Y., & Xia, J. (2017). Iron oxide nanoparticles with different polymer coatings for photothermal therapy. *Journal of Nanoparticle Research*, *19*(10), 333. https://doi.org/10.1007/s11051-017-4031-3

Zhou, B., Li, Y., Niu, G., Lan, M., Jia, Q., & Liang, Q. (2016). Near-Infrared Organic Dye-Based Nanoagent for the Photothermal Therapy of Cancer. *ACS Applied Materials & Interfaces*, *8*(44), 29899–29905. https://doi.org/10.1021/acsami.6b07838